

An optimal h - and r - adaptive strategy in L^2 and L^∞ norm to the Poisson equation on non-convex domains

Simone Appella, Chris Budd and Tristan Pryer

August 30, 2021

Abstract

In this paper, we investigate the properties of h - and r -adaptive mesh strategies for the numerical solution of the Poisson equation, discretised with the discontinuous Galerkin method, on non-convex domains. To drive the mesh adaptation, we derive a *novel a-posteriori estimator* by using the theoretical framework of weighted Sobolev spaces and the duality argument. A L^∞ a-posteriori bound will be also used in the numerical experiments, which will evidence optimal convergence property for both estimators. Concerning the r -adaptive methods, we will show that a parameter-dependent Optimal Transport strategy is able to outperform the Winslow' Moving mesh PDE method in terms of accuracy and quality of the mesh. The parameter that numerically provides the highest accuracy is justified by a theoretical argument. Furthermore, we will prove and provide numerical proof that that optimal *OT mesh equidistributes the a-posteriori estimators in both norms*, hinting at the similarities between the r - and h -adaptation process. Finally, we will prove and show numerically that the *mesh skewness*, another quality measure for r -adaptive meshes, does only depend on the re-entrant corner and not on the degrees of freedom of the mesh.

1 Introduction

Solutions of elliptic boundary value problems defined on non-convex domains display singular behaviour near re-entrant corners. This occurs even when data of the underlying problem are very smooth. Such singular behaviour affects the accuracy of Finite Element Methods (FEMs) throughout the whole domain. Hence, the solutions of the corresponding problems lie typically in Sobolev spaces H^k for small $k > 1$ [BG88; BG89]. The theoretical framework of weighted Sobolev spaces, which were originally studied in [BR72; BKP79] for elasticity and potential problems, will be employed throughout the paper for discretising the Poisson equation and providing the tools for the derivation of an L^2 -based a-posteriori bound.

We treat the equation defined on a general non-convex domain with prescribed Dirichlet boundary conditions. The numerical solution of this equation has been already addressed in [ZSG02; SH16; ZS02]. The discretisation is performed with the Symmetric Interior Penalty discontinuous Galerkin (SIP-dG) method, formulated in [Arn82; Arn+00; Arn+02] and extended to solve general convection-diffusion problems [CC98; CC01]. The popularity of the dG method resides in its flexibility with respect to adapted elements of various types and shapes. Though, in all the previous works, error estimates of h - or p -type under strong regularity assumptions are given. In order to resolve the singularities, appropriate adaptive mesh strategies must be carefully selected in order to obtain the optimal order of convergence.

Our first contribution consists in the derivation of an *a-posteriori* estimate in the L^2 norm with one re-entrant corner. The proof relies on the dual weak dual formulation of the Poisson problem, inspired by the work in [Wih03; Sch98].

The derivation of the a-posteriori estimator is based on the following steps:

- State the Poisson problem with non-homogeneous Dirichlet and/or Neumann boundary conditions. Claim existence and uniqueness of the solution using the framework of the weighted Sobolev spaces.
- Define the SIP-dG variational formulation of the Poisson problem.
- State consistency of the SIP-dG method and the resulting Galerkin orthogonality with respect to the dG space.
- Formulate the weak dual problem of the Poisson equation with the error as given datum and derive the corresponding SIP-dG variational formulation.
- Define a proper interpolant of the solution of the dual problem and exploit the Galerkin orthogonality, interpolation bounds, and regularity results [BG88] to obtain the a-posteriori estimate.

In §4, the adapted SIP-dG method will be tested for different adaptive strategies on the L-shaped and crack domain. The rate of convergence in the L^2 and L^∞ norm for the h -refinement will be computed using the corresponding a-posteriori bounds, where in the latter case the expression is provided in [DG12]. As r -adaptive methods, the Winslow's Moving Mesh PDE (MMPDE) and an Optimal Transport (OT) strategy will be employed. We will mainly focus on the properties of the OT mesh, as the former method performs poorly in terms of accuracy, quality of the mesh, and computational complexity. We will show that both h -refinement and OT mesh yield *optimal order of convergence* in the two norms.

As further contribution to this paper we investigate in detail the relationship between the OT mesh and equidistribution of the a-posteriori estimator. We will first evidence how a parameter, used in the OT mesh generation, will affect its quality and the accuracy of the numerical solver. We will then prove, both theoretically and numerically, that the OT mesh yielding highest accuracy in a specific norm is able to equidistribute the corresponding a-posteriori bound in the vicinity of the corner.

Finally, we address the question of how to assess the quality of the mesh resulting from the OT method using the *Skewness* metric. We will show that this quantity does only depend on the re-entrant corner and not on the dimension of the FE space. The theoretical proof is corroborated by numerical tests.

The remainder of the paper is structured as follows. In §2 we introduce the notation and the theory to derive the SIP-dG discretisation of the Poisson equation. In §3 we derive an a-posteriori error estimator in the L^2 norm from the weak dual formulation of the original problem. In §4 we discuss accuracy and quality measure of the mesh obtained through h - r -adaptation and provide numerical evidence of the properties mentioned in the previous paragraph.

Finally, we will draw our conclusions and propose ideas to further expand this work in §6.

2 Problem setup and discretisation

Let $\Omega \subset \mathbb{R}^2$ be a bounded, polygonal domain with outward unit normal \vec{n}_Ω . Suppose that the boundary $\Gamma = \partial\Omega$ is composed by a Dirichlet part Γ_D with $|\Gamma_D| > 0$ and a Neumann part Γ_N such that:

$$\bar{\Gamma} = \bar{\Gamma}_D \cup \bar{\Gamma}_N. \quad (1)$$

All the vertices are included in the closure. The corner vertices and the points of changing boundary conditions are *singular points* and collected in the set

$$SP(\Omega, \Gamma_D, \Gamma_N) = \{A_i : i = 1, \dots, M\}. \quad (2)$$

The interior opening angle of the domain at A_i is measured anti-clockwise and denoted by $\omega \in (0, 2\pi]$. The case $\omega = \pi$ allows boundary conditions to switch from Neumann to Dirichlet or vice versa.

To account for the regularity of the elliptic problem, suitable Sobolev spaces will be introduced. A weight $\beta_i \in (0, 1]$ is associated with each singular point $A_i \in SP(\Omega, \Gamma_D, \Gamma_N)$ and stored in the vector $\vec{\beta} = (\beta_1, \dots, \beta_M)$. For any number $k \in \mathbb{R}$, we let

$$\vec{\beta} + k = (\beta_1 + k, \dots, \beta_M + k).$$

We then introduce the weight function on Ω :

$$\Phi_{\vec{\beta}}(\vec{x}) = \prod_{i=1}^M r_i(\vec{x})^{\beta_i}, \quad r_i(\vec{x}) = |\vec{x} - A_i|.$$

Then, for any integers $m \geq l \geq 0$, the weighted Sobolev spaces $H_{\vec{\beta}}^{m,l}(\Omega)$ are defined as completion of the space $C^\infty(\overline{\Omega})$ with respect to the weighted Sobolev norms

$$\begin{aligned} \|u\|_{H_{\vec{\beta}}^{m,l}(\Omega)}^2 &= \|u\|_{H^{l-1}(\Omega)}^2 + |u|_{H_{\vec{\beta}}^{m,l}(\Omega)}^2, \quad l \geq 1 \\ \|u\|_{H_{\vec{\beta}}^m(\Omega)}^2 &= \sum_{|\alpha|=k}^m \left\| |D^\alpha u| \Phi_{\vec{\beta}+k} \right\|_{L^2(\Omega)}^2, \quad l=0, \end{aligned} \tag{3}$$

where

$$|u|_{H_{\vec{\beta}}^{m,l}(\Omega)}^2 = \sum_{\substack{|\alpha|=k \\ k=l}}^m \left\| |D^\alpha u| \Phi_{\vec{\beta}+k-l} \right\|_{L^2(\Omega)}^2$$

and

$$D^\alpha u = \frac{\partial^{|\alpha|} u}{\partial x_1^{\alpha_1} \partial x_2^{\alpha_2}},$$

with $\alpha = (\alpha_1, \alpha_2) \in \mathbb{N}^2$ and $|\alpha| = \alpha_1 + \alpha_2$.

Fractional Sobolev spaces for $m \in \mathbb{R}$ appear naturally as the correct range of the continuous trace map

$$\tau : H^m(\Omega) \rightarrow H^{m-1/2}(\Gamma), \quad m > 1/2,$$

and will be used to define properly the boundary conditions for the Poisson problem.

We mention the following remark proved in [Wih03]:

Remark 1 (Properties of the weighted Sobolev spaces [Wih03, Remark 1.2.2]) *The following properties hold:*

1. If $u \in H_{\vec{\beta}}^{m,m}(\Omega)$, $m \geq 0$, then $u \in H^m(\Omega_0)$ for all domains $\Omega_0 \subset \Omega$ with

$$P \notin \overline{\Omega_0} \quad \forall P \in SP(\Omega, \Gamma_D, \Gamma_N).$$

2. Although $H_{\vec{\beta}}^{2,2}(\Omega) \not\subset H^2(\Omega)$, it was proven in [BKP79] that $H_{\vec{\beta}}^{2,2}(\Omega) \subset \mathcal{C}^0(\overline{\Omega})$.
3. For $u \in H_{\vec{\beta}}^{2,2}(\Omega)$, there holds $\nabla u \in H_{\vec{\beta}}^{1,1}(\Omega)^2$.

2.1 Poisson equation in 2D

Let $\Omega \subset \mathbb{R}^2$ be a bounded, polygonal domain. Consider the following *Poisson problem*

$$\begin{aligned} -\Delta u &= f \text{ in } \Omega \\ u &= u_D \text{ on } \Gamma_D \\ \nabla u \cdot \vec{n}_\Omega &= g \text{ on } \Gamma_N. \end{aligned} \tag{4}$$

Here, f is a given datum lying on the dual space of $H_0^1(\Omega)$ and denoted by $H^{-1}(\Omega)$, $u_D \in H^{1/2}(\Gamma_D)$ and $g \in H^{-1/2}(\Gamma_N)$ are prescribed Dirichlet and Neumann boundary conditions, respectively. In the framework of weighted Sobolev spaces, the existence and uniqueness of problem (4) is stated in the following Theorem:

Theorem 2 (Regularity of the Poisson equation [BG88, Theorem 3.1]) *Let Ω be a polygon in \mathbb{R}^2 and $m \geq 0$ a given integer. Then, there exists a weight vector $\vec{\beta}_{min}$ with $0 \leq \vec{\beta}_{min} < 1$ depending on the opening angles at the vertices $A_i \in SP(\Omega, \Gamma_D, \Gamma_N)$, such that for weight vectors $\vec{\beta}$ with $\vec{\beta}_{min} \leq \vec{\beta} < 1$ and for*

$$f \in H_{\vec{\beta}}^{m,0}(\Omega), u_D \in H_{\vec{\beta}}^{m+3/2,3/2}(\Gamma_D), g \in H_{\vec{\beta}}^{m+1/2,1/2}(\Gamma_N),$$

the problem (4) has a unique solution $u \in H_{\vec{\beta}}^{m+2,2}(\Omega)$.

Remark 3 ([BG88, Theorem 2.1 - Remark 3]) *In the case of the Poisson equation the value of $\vec{\beta}_{min}$ is well-known at each corner A_i and given by*

$$\beta_{min,i} = \begin{cases} 1 - \frac{\pi}{\omega} & \text{if } \overline{A_i A_{i+1}} \in \Gamma_D \text{ or } \Gamma_N, \\ 1 - \frac{\pi}{2\omega} & \text{otherwise.} \end{cases} \tag{5}$$

2.2 Finite element spaces

Let \mathcal{T} be a conforming mesh of Ω into simplicial open elements K :

$$\mathcal{T} = \{K_i\}_i, \quad \bigcup_{K \in \mathcal{T}} \overline{K} = \overline{\Omega}.$$

We consider \mathcal{T} is a finite family of sets such that:

1. $K \in \mathcal{T}$ implies K is an open triangle or quadrilateral,
2. for any $K, J \in \mathcal{T}$ we have that $\overline{K} \cap \overline{J}$ is either empty or a complete $(2-r)$ -dimensional simplex/box (i.e., it is either a vertex for $r=2$, or an edge for $r=1$, or the whole of \overline{K} and \overline{J} of both \overline{K} and \overline{J} ,
3. $\bigcup_{K \in \mathcal{T}} \overline{K} = \overline{\Omega}$.

Additionally, for each $K \in \mathcal{T}$ we introduce

$$h_K = diam(K) := \sup_{x,y \in K} |x - y|$$

and

$$\rho_K = \sup\{diam(B) : B \text{ is an open ball contained in } K\}.$$

Finally, the maximum and minimum *mesh width* of \mathcal{T} is given by

$$\bar{h} = \max_{K \in \mathcal{T}} h_K, \quad \underline{h} = \min_{K \in \mathcal{T}} h_K.$$

We will also assume that all the meshes generated by the h -, r - refinement are *shape regular*. Let $\mathcal{G} = \{\mathcal{T}_i\}_{i \in \mathbb{N}}$ be a family of meshes, then \mathcal{G} is characterised by the shape regularity $\mu(\mathcal{T})$ if

$$\mu(\mathcal{T}) = \min_{K \in \mathcal{T}_i} \frac{h_K}{\rho_K} > 0. \quad (6)$$

The set of all edges of \mathcal{T} is denoted by \mathcal{E} , which we partition into subsets $\mathcal{E}_D, \mathcal{E}_N, \mathcal{E}_I$, consisting of edges lying on the Dirichlet boundary Γ_D , the Neumann boundary Γ_N , and the interior edges, respectively. The corresponding quantities for each individual element K are denoted by $\mathcal{E}(K), \mathcal{E}_D(K), \mathcal{E}_N(K), \mathcal{E}_I(K)$, respectively.

We split the index set $\{1, \dots, M\}$ of boundary edges e_i into \mathcal{D} and \mathcal{N} , on which Dirichlet and Neumann boundary conditions are applied, respectively. This leads to $\bar{\Gamma}_D = \bigcup_{i \in \mathcal{D}} \bar{e}_i$ and $\bar{\Gamma}_N = \bigcup_{i \in \mathcal{N}} \bar{e}_i$.

We define the *finite element space*

$$\mathbb{V} := \{v \in L^2(\Omega) : v|_K \in \mathbb{P}^p(K) \quad \forall K \in \mathcal{T}\}, \quad (7)$$

where $\mathbb{P}^p(K)$ is the space of polynomials of total degree p .

We remark that the space \mathbb{V} does not carry any inter-element continuity and does not encode any boundary condition. These will be enforced weakly in the variational scheme. Given an edge γ of \mathcal{T} , we define the *jump* and *average* operator of $v \in \mathbb{V}$ on the edges \mathcal{E} at $\vec{x} \in \gamma$ by

$$[\![v]\!] := \begin{cases} v|_K \vec{n}_K + v|_{K'} \vec{n}_{K'} & \text{on } \gamma = \partial K \cap \partial K' \\ v|_K \vec{n}_\Omega & \text{on } \gamma = \partial K \cap \Gamma_D \end{cases} \quad [\![\vec{v}]\!] := \begin{cases} \vec{v}|_K \cdot \vec{n}_K + \vec{v}|_{K'} \cdot \vec{n}_{K'} & \text{on } \gamma = \partial K \cap \partial K' \\ \vec{v}|_K \cdot \vec{n}_\Omega & \text{on } \gamma = \partial K \cap \Gamma_D \end{cases} \quad (8)$$

$$\{\!\!\{ v \}\!\!\} := \begin{cases} \frac{1}{2}(v|_K + v|_{K'}) & \text{on } \gamma = \partial K \cap \partial K' \\ v|_K & \text{on } \gamma = \partial K \cap \Gamma_D \end{cases} \quad \{\!\!\{ \vec{v} \}\!\!\} := \begin{cases} \frac{1}{2}(\vec{v}|_K + \vec{v}|_{K'}) & \text{on } \gamma = \partial K \cap \partial K' \\ \vec{v}|_K & \text{on } \gamma = \partial K \cap \Gamma_D \end{cases} \quad (9)$$

Here $v|_K$ denotes the trace of v onto the edge $\gamma \in \mathcal{E}(K) \cap \mathcal{E}(K')$ and \vec{n}_K is the outward unit vector relative to K on γ . For $\gamma \subset \Gamma$, we define $\{\!\!\{ v \}\!\!\} := v$, $\{\!\!\{ \vec{v} \}\!\!\} := \vec{v}$, $[\![v]\!] := v \vec{n}_\Omega$, and $[\![\vec{v}]\!] := \vec{v} \cdot \vec{n}_\Omega$.

Using the jump and average operator we introduce the mesh condition $q(\mathcal{T})$ as an alternative quality measure. Under the condition

$$q := \|[\![h]\!]/\{\!\!\{ h \}\!\!\}\|_{L^\infty(\mathcal{E}_I)} \leq \alpha, \quad 0 \leq \alpha < 1 \text{ small enough,} \quad (10)$$

it has been shown that the inf-sup stability of the bilinear form given by the weak formulation of the Poisson equation holds [GMP17].

To account for the singular behaviour of solutions near singular points of the polygon Ω , we define the set

$$\mathcal{K}_0 = \{K \in \mathcal{T} : P \in \bar{K} \text{ for some } P \in SP(\Omega, \Gamma_D, \Gamma_N)\}. \quad (11)$$

Let $K \in \mathcal{K}_0$. We will assume the mesh is graded enough such that exactly one singular point belongs to \bar{K} . The corresponding vertex is denoted by A_K and the corresponding weight β_K . Moreover, the spaces $H_{\beta_K}^{m,l}(K)$ are equipped with the weight function $\Phi_{\beta_K}(\vec{x}) = r_K^{\beta_K}$, where $r_K = |\vec{x} - A_K|$.

We conclude the section by stating the following lemmas [Wih03]:

Lemma 4 (Trace inequalities [Wih03, Lemma A.2.4]) *Let $\gamma \in \mathcal{E}(K)$. Then, there holds*

1. if $u \in H^2(K)$ and $u = 0$ at the vertices of K , then the trace $u|_\gamma \in H^1(\gamma)$ and

$$\begin{aligned} \|u\|_{H^1(\gamma)}^2 &\leq Ch_K |u|_{H^2(K)}^2 \\ \|u\|_{L^2(\gamma)}^2 &\leq Ch_K^3 |u|_{H^2(K)}^2. \end{aligned} \quad (12)$$

2. if $u \in H_{\vec{\beta}}^{2,2}(\Omega)$, $0 < \beta < 1$, and $u = 0$ at the vertices of K , then

$$\begin{aligned}\|u\|_{H^1(\gamma)}^2 &\leq Ch_K^{1-2\beta}|u|_{H_{\vec{\beta}}^{2,2}(K)}^2 \\ \|u\|_{L^2(\gamma)}^2 &\leq Ch_K^{3-2\beta}|u|_{H_{\vec{\beta}}^{2,2}(K)}^2,\end{aligned}\tag{13}$$

if γ does not contain any vertex A_i , $i = 1, \dots, M$.

Lemma 5 (Continuity at the interior edges [Wih03, Lemma 1.3.4]) Let $u \in H_{\vec{\beta}}^{1,1}(\Omega)$ for $0 \leq \vec{\beta} \leq 1$. Then, for an interior edge $\gamma \in \mathcal{E}_I$ there holds $\llbracket u \rrbracket = 0$ a.e. on γ .

2.3 Variational formulation of the Poisson equation

Here, we define the SIP-dG variational formulation of problem (4) and state its consistency.

Definition 2.1 (SIP-dG of the Poisson equation) Define the bilinear form \mathcal{A}_h by

$$\begin{aligned}\mathcal{A}_h(u, v) := & \sum_{K \in \mathcal{T}} \int_K \nabla_h u \cdot \nabla_h v \, d\vec{x} \\ & - \sum_{\gamma \in \mathcal{E}_I \cup \mathcal{E}_D} \int_\gamma (\llbracket v \rrbracket \cdot \{ \nabla_h u \} + \llbracket u \rrbracket \cdot \{ \nabla_h v \}) \, ds \\ & + \sum_{\gamma \in \mathcal{E}_I \cup \mathcal{E}_D} \int_\gamma \sigma \llbracket u \rrbracket \cdot \llbracket v \rrbracket \, ds,\end{aligned}\tag{14}$$

and the corresponding linear functional l_h by

$$l_h(v) := \sum_{K \in \mathcal{T}} \int_K f v \, d\vec{x} + \int_{\Gamma_N} g v \, ds - \sum_{\gamma \in \mathcal{E}_D} \int_\gamma (\nabla_h v \cdot \vec{n}_\Omega) u_D \, ds + \sum_{\gamma \in \mathcal{E}_D} \frac{\sigma}{|\gamma|} \int_\gamma u_D v \, ds,\tag{15}$$

where $\sigma := C_\sigma 1/h > 0$ is the, so called, discontinuity penalisation parameter. The constant $C_\sigma > 0$ is typically chosen large enough so as to achieve coercivity.

Then, the SIP-dG method of the Poisson problem (4) reads as: Find $u_h \in \mathbb{V}$ such that

$$\mathcal{A}_h(u_h, v_h) = l_h(v_h) \quad \forall v_h \in \mathbb{V}.\tag{16}$$

Some basic properties of the SIP-dG method, such as existence and uniqueness of the result, have been proved in [Wih03]. In particular, we are interested in the subsequent analysis to the following proposition:

Proposition 6 (Consistency of the SIP-dG method) For $f \in H_{\vec{\beta}}^{0,0}(\Omega)$, $u_D \in H_{\vec{\beta}}^{3/2,3/2}(\Gamma_D)$, $g \in H_{\vec{\beta}}^{1/2,1/2}(\Gamma_N)$, the bilinear form and the linear functional in Definition 2.1 are well-defined and the SIP-dG method is consistent:

$$\mathcal{A}_h(u, v_h) - l_h(v_h) = 0 \quad \forall v_h \in \mathbb{V},\tag{17}$$

where $u \in H_{\vec{\beta}}^{2,2}(\Omega)$ is the exact solution of (4). Let $e = u - u_h$ be the error in the SIP-dG method. Using the previous result the following Galerkin orthogonality holds:

$$\mathcal{A}_h(e, v_h) = 0 \quad \forall v_h \in \mathbb{V}.\tag{18}$$

3 A-posteriori error estimate of the SIP-dG method

In this section, we derive the a-posteriori bound in the L^2 used for both h- and r-adaptive strategies in the subsequent numerical experiments.

We consider the dual problem of (4):

$$\begin{aligned} -\Delta\phi &= e \text{ in } \Omega \\ \phi &= 0 \text{ on } \Gamma. \end{aligned} \tag{19}$$

Since $e \in \mathbb{V} \subset H_{\vec{\beta}}^{0,0}(\Omega)$, the conditions of Theorem 2 are satisfied and the problem (19) admits a (weak) solution $\phi \in H_{\vec{\beta}}^{2,2}(\Omega)$. Moreover

$$\mathcal{A}_h(\phi, v_h) = l_h(v_h) = \langle e, v \rangle_{L^2(\Omega)} \quad \forall v_h \in \mathbb{V}, \tag{20}$$

where $\langle \cdot, \cdot \rangle_{L^2(\Omega)}$ on right hand side (rhs) denotes the standard inner product in $L^2(\Omega)$. This can be used for the derivation of general goal oriented estimators, which can affect the properties of the resulting adapted mesh. We now state the following proposition and lemmas, that will be used for the derivation of the L^2 a-posteriori error estimator:

Proposition 7 (Regularity of the solution on weighted Sobolev Spaces) *Due to Theorem 2.1 [BG88], if $e \in H_{\vec{\beta}}^{k,0}(\Omega)$, for $k \geq 0$, there exists $\phi \in H_{\vec{\beta}}^{k+2,2}(\Omega)$, where $\vec{\beta}$ depends on the opening angles at the vertices of Ω , such that*

$$\|\phi\|_{H_{\vec{\beta}}^{k+2,2}(\Omega)} \leq C(k) \|e\|_{H_{\vec{\beta}}^{k,0}(\Omega)}. \tag{21}$$

Since $e \in \mathbb{V} \subset H_{\vec{\beta}}^{2,2}(\Omega)$, we can take $k = 0$ and exploit Remark (1) to obtain

$$\|\phi\|_{H_{\vec{\beta}}^{2,2}(\Omega)} \leq C \|e\|_{L^2(\Omega)}. \tag{22}$$

Lemma 8 (Nodal interpolants for dG-FEM) *For an element $K \in \mathcal{T}/\mathcal{K}_0$, let $\Pi_K : \mathcal{C}^0(\bar{K}) \rightarrow \mathcal{P}^1(K)$ denote the piece-wise linear operator into polynomials of degree at most one. By standard interpolation results [BS08] there holds*

$$\|v - \Pi_K v\|_{L^2(K)} \leq Ch_K \|v\|_{H^1(K)}. \tag{23}$$

In corner elements $K \in \mathcal{K}_0$, the interpolation bounds in [Wih03; Sch98] (Lemma 2.5.3.) for the linear interpolant in the weighted space $H_{\vec{\beta}}^{2,2}(K)$ for $\beta_K \in [0, 1]$ gives

$$\|v - \Pi_K v\|_{H^1(K)} \leq Ch_K^{1-\beta_K} \|v\|_{H_{\beta_K}^{2,2}(K)}. \tag{24}$$

Lemma 9 (Discrete trace inequality [EG21]) *Assuming that $P \subset L^\infty(K)$, there exists a constant c such that the following holds:*

$$\|v\|_{L^p(F, \mathbb{R}^n)} \leq c h_K^{-\frac{1}{p} + n(\frac{1}{p} - \frac{1}{r})} \|v\|_{L^r(K, \mathbb{R}^n)}, \tag{25}$$

for all $p, r \in [1, \infty]$, all $v \in P_K$, all $K \in \mathcal{T}$, and all the faces F of K .

We can now proceed with the derivation of the estimator. We start by taking $v_h = e$ in equation (20) and exploit the Galerkin orthogonality for the linear interpolant $\Pi_h v$, defined as $\Pi_h v|_K = \Pi_K v$. We have that $\Pi_K v \subset \mathcal{C}^0(K) \subset \mathbb{V}$. Then, using the Galerkin orthogonality (18)

$$\begin{aligned} \|e\|_{L^2(\Omega)}^2 &= \mathcal{A}_h(\phi, e) = \mathcal{A}_h(\phi - \Pi_h \phi, e) = \sum_{K \in \mathcal{T}} \int_K \nabla_h(\phi - \Pi_h \phi) \cdot \nabla_h e \, d\vec{x} \\ &\quad - \sum_{\gamma \in \mathcal{E}_I} \int_\gamma (\llbracket \phi - \Pi_h \phi \rrbracket \cdot \llbracket \nabla_h e \rrbracket + \llbracket e \rrbracket \cdot \llbracket \nabla_h(\phi - \Pi_h \phi) \rrbracket) \, ds. \end{aligned} \tag{26}$$

Integration by parts of the first term on the rhs gives

$$\begin{aligned}\|e\|_{L^2(\Omega)}^2 &= \sum_{K \in \mathcal{T}} \int_K (\phi - \Pi_h \phi)(f + \Delta_h u_h) d\vec{x} \\ &\quad + \sum_{\gamma \in \mathcal{E}_I} \int_\gamma \left((\phi - \Pi_h \phi) [\nabla_h u_h] + [u_h] \cdot \{\nabla_h(\phi - \Pi_h \phi)\} \right) ds,\end{aligned}$$

where we have also exploited Remark 1 and Lemma 5 on u and $\nabla_h u$, respectively.
We then apply the Cauchy-Schwartz inequality:

$$\begin{aligned}\|e\|_{L^2(\Omega)}^2 &\leq \sum_{K \in \mathcal{K}_0} \|\phi - \Pi_h \phi\|_{L^2(K)} \|f + \Delta_h u_h\|_{L^2(K)} + \sum_{K \in \mathcal{T}/\mathcal{K}_0} \|\phi - \Pi_h \phi\|_{L^2(K)} \|f + \Delta_h u_h\|_{L^2(K)} \\ &\quad + \sum_{\gamma \in \mathcal{E}_I} \|\phi - \Pi_h \phi\|_{L^2(\gamma)} \|[\nabla_h u_h]\|_{L^2(\gamma)} + \sum_{\gamma \in \mathcal{E}_I} \| [u_h] \|_{L^2(\gamma)} \|\nabla_h \{\phi - \Pi_h \phi\}\|_{L^2(\gamma)}. \tag{27}\end{aligned}$$

For the first term we have by Lemma 8 and Proposition 7 that

$$\|\phi - \Pi_h \phi\|_{L^2(K)} \leq Ch_K \|\phi - \Pi_h \phi\|_{H^1(K)} \leq Ch_K^{2-\beta_K} |\phi|_{H_{\beta}^{2,2}(\Omega)} \leq Ch_K^{2-\beta_K} \|e\|_{L^2(\Omega)} \quad \forall K \in \mathcal{K}_0. \tag{28}$$

For the second term, Lemma 8 gives

$$\|\phi - \Pi_h \phi\|_{L^2(K)} \leq Ch_K^2 |\phi|_{H^2(K)} \leq Ch_K^2 \|e\|_{L^2(\Omega)} \quad \forall K \in \mathcal{T}/\mathcal{K}_0. \tag{29}$$

For the remaining two terms we have:

$$\begin{aligned}\|\phi - \Pi_K \phi\|_{L^2(\gamma)} &\leq C\sqrt{h_K} \|\phi - \Pi_K \phi\|_{H^1(K)} \\ &\leq \begin{cases} Ch_K^{3/2-\beta_K} \|\phi\|_{H_{\beta_K}^{2,2}(K)} \leq Ch_K^{3/2-\beta_K} \|e\|_{L^2(\Omega)} & \text{if } \gamma \in K \in \mathcal{K}_0, \\ Ch_K^{3/2} \|\phi\|_{H^2(K)} \leq Ch_K^{3/2} \|e\|_{L^2(\Omega)} & \text{if } \gamma \in K \notin \mathcal{K}_0. \end{cases} \tag{30}\end{aligned}$$

Using Lemma 9 we obtain the upper bound:

$$\begin{aligned}\|\{\nabla_h(\phi - \Pi_K \phi)\}\|_{L^2(\gamma)} &\leq Ch_K^{-1/2} \|\nabla_h(\phi - \Pi_K \phi)\|_{L^2(K)} \\ &\leq h_k^{-1/2} \|\phi - \Pi_K \phi\|_{H^1(K)} \\ &\leq \begin{cases} Ch_k^{1/2-\beta_K} \|e\|_{L^2(\Omega)} & \text{if } \gamma \in K \in \mathcal{K}_0, \\ Ch_k^{1/2} \|e\|_{L^2(\Omega)} & \text{if } \gamma \in K \notin \mathcal{K}_0. \end{cases} \tag{31}\end{aligned}$$

Replacing the results obtained in (28)-(31) in equation (27) we have:

$$\begin{aligned}\|e\|_{L^2(\Omega)} &\leq C_1 \sum_{K \in \mathcal{K}_0} \left(h_K^{2-\beta_K} \|f + \Delta_h u_h\|_{L^2(K)} + \right. \\ &\quad \left. \frac{1}{2} \sum_{\partial K \in \mathcal{E}(K)} (h_K^{3/2-\beta_K} \|\nabla_h u_h\|_{L^2(\partial K)} + h_K^{1/2-\beta_K} \|u_h\|_{L^2(\partial K)}) \right) \\ &\quad + C_2 \sum_{K \in \mathcal{T}/\mathcal{K}_0} \left(h_K^2 \|f + \Delta_h u_h\|_{L^2(K)} + \frac{1}{2} \sum_{\partial K \in \mathcal{E}(K)} (h_K^{3/2} \|\nabla_h u_h\|_{L^2(\partial K)} + h_K^{1/2} \|u_h\|_{L^2(\partial K)}) \right). \tag{32}\end{aligned}$$

This expression can be simplified if $u \in \mathbb{V}$ with $p = 1$ and $f = 0$. We further introduce the indicator function $\mathbb{1}_{\gamma \in \mathcal{E}_I(\mathcal{K}_0)}$ and rewrite (32) in the more compact form

$$\begin{aligned} \|e\|_{L^2(\Omega)} &\leq \sum_{\gamma \in \mathcal{E}_I} (h_{K(\gamma)}^{3/2-\mathbb{1}_{\gamma \in \mathcal{E}_I(\mathcal{K}_0)}\beta_\gamma} \|\llbracket \nabla_h u_h \rrbracket\|_{L^2(\gamma)} + h_{K(\gamma)}^{1/2-\mathbb{1}_{\gamma \in \mathcal{E}_I(\mathcal{K}_0)}\beta_\gamma} \|\llbracket u_h \rrbracket\|_{L^2(\gamma)}) \\ &\leq \left(\sum_{\gamma \in \mathcal{E}_I} h_{K(\gamma)}^{3-\mathbb{1}_{\gamma \in \mathcal{E}_I(\mathcal{K}_0)}2\beta_\gamma} \|\llbracket \nabla_h u_h \rrbracket\|_{L^2(\gamma)}^2 + h_{K(\gamma)}^{1-\mathbb{1}_{\gamma \in \mathcal{E}_I(\mathcal{K}_0)}2\beta_\gamma} \|\llbracket u_h \rrbracket\|_{L^2(\gamma)}^2 \right)^{1/2}. \end{aligned} \quad (33)$$

For practical purposes, we reformulate (33) for each K in order to obtain a cell-wise error indicator:

$$\|e\|_{L^2(\Omega)}^2 \leq \sum_{K \in \mathcal{T}} \sum_{\gamma \in \mathcal{E}_I(K)} h_K^{3-\mathbb{1}_{\gamma \in \mathcal{E}_I(\mathcal{K}_0)}2\hat{\beta}_\gamma} \|\llbracket \nabla_h u_h \rrbracket\|_{L^2(\gamma)}^2 + h_K^{1-\mathbb{1}_{\gamma \in \mathcal{E}_I(\mathcal{K}_0)}2\hat{\beta}_\gamma} \|\llbracket u_h \rrbracket\|_{L^2(\gamma)}^2, \quad (34)$$

where $\hat{\beta} \in [0, 1]$ replaces the weight β , whose range is specified in Remark 3. Here, actually, $\hat{\beta}$ defines an upper bound for the L^2 error and does not prevent the solution u of problem 4 to lie in an admissible weighted Sobolev space.

We conclude this section by presenting an L^∞ a-posteriori estimator for the SIP-dG method [DG12]. The domain Ω is not required to be Lipschitz, thus the following bound can be tested for our numerical experiments:

$$\|u - u_h\|_{L^\infty(\Omega)} \leq Cl_{h,d} \left(\|h^2(f + \Delta_h u_h)\|_{L^\infty(\Omega)} + \|h \llbracket \nabla u_h \rrbracket\|_{L^\infty(\mathcal{E}_I)} + \|\llbracket u_h \rrbracket\|_{L^\infty(\mathcal{E}_I)} + \|u_D - u_h\|_{L^\infty(\partial\Omega)} \right), \quad (35)$$

where $l_{h,d} = (\ln 1/\underline{h})^2$.

4 Numerical Results

In this section we consider as model problem the Poisson equation

$$\begin{aligned} -\Delta u &= 0 \text{ in } \Omega \\ u_D(r, \theta) &= r^{\pi/\omega} \sin(\pi\theta/\omega) \text{ on } \Gamma, \end{aligned} \quad (36)$$

where $\omega \in (\pi, 2\pi)$ is the angle of the re-entrant corner located at $\vec{0} = (0, 0) \in \mathbb{R}^2$. We evidence that u is analytic in $\overline{\Omega}/\{\vec{0}\}$ and $u \notin H^2(\Omega)$, so that $SP(\Omega, \Gamma_D, \Gamma_N) = \{A_1 := \vec{0}\}$. Therefore, the weight function is defined as $\Phi_\beta(\vec{x}) = |\vec{x}|^\beta$, where $\beta \in (1 - \frac{\pi}{\omega}, 1]$, according to Remark 3. Let Ω be the L-shaped domain $(-1, 1)^2/[0, 1] \times (-1, 0]$. Then, the harmonic solution of problem (36) is

$$u(r, \theta) = r^{2/3} \sin(2\theta/3). \quad (37)$$

We compare the accuracy of the SIP-dG method applied to problem (36) using different adaptive mesh strategies and assess the quality of the resulting meshes. For all the tests, we compute the numerical solution $u_h \in \mathbb{V}$ with $p = 1$. All the tests have been performed in FEniCS [LW10].

4.1 h-refinement

In the h -adaptive process, we introduce the global error indicator $\eta^2 = \sum_{K \in \mathcal{T}} \eta_K^2$, where η_K^2 refers to each cell K on the rhs of equation (34). As a widely accepted criterion, elements with large error estimator should be marked for refinement. Here, we employ the so called *maximum strategy* (*ms*), which can be described as follows

$$\eta_K \geq \alpha \max_{K' \in \mathcal{T}} \eta_{K'} \iff K \text{ is marked for refinement}, \quad (38)$$

where $\alpha \in (0, 1)$ is a predetermined parameter. The steps involved in the ms h -refinement are given below:

1. Compute the error indicators $\{\eta_K \mid K \in \mathcal{T}\}$ for each cell according to equation (34).
2. Mark elements for refinement using equation (38).
3. Refine each marked element by edge bisection.

The same procedure is applied for the L^∞ a-posteriori bound, denoted by $\tilde{\eta}_K$.

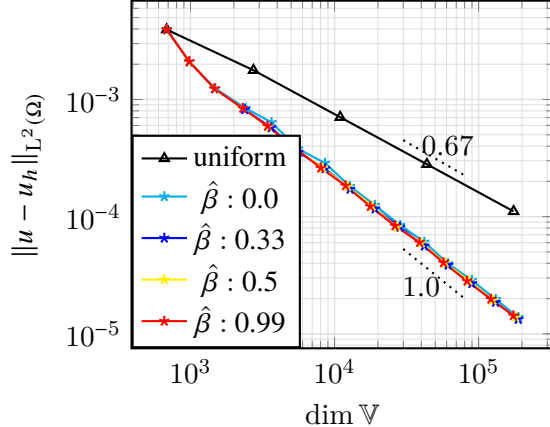


Figure 1: Asymptotic convergence rates for the h-refinement strategy on the finite element space \mathbb{V} . Note that the rate of convergence is optimal and independent on $\hat{\beta}$. Uniform mesh refinement yields a convergence rate of $2/3$ due to the singular behaviour of the solution near the origin [GMP17].

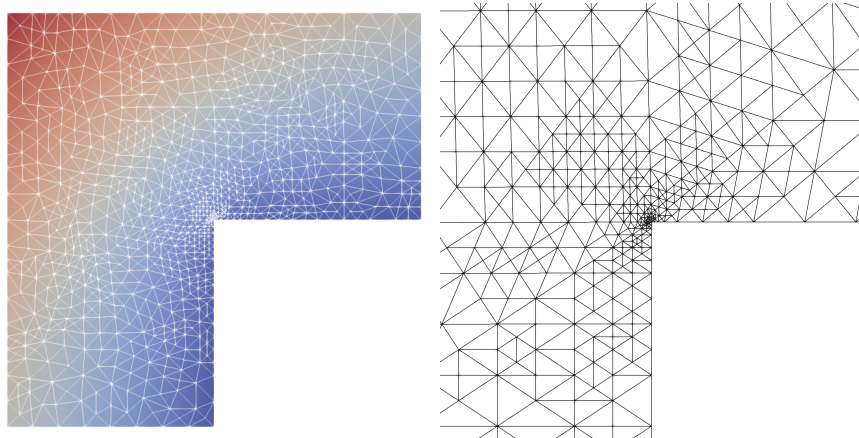


Figure 2: (Left) Solution of eq.(36) obtained via the L^∞ a-posteriori bound (35) after 15 refinements. (Right) Zoom of the mesh on the re-entrant corner.

The ms h -refinement strategy with $\alpha = 0.1$ has been tested for different $\hat{\beta}$. As visible in Fig.3, the level of refinement is increasing near the corner as a function of $\hat{\beta}$. It appears from Fig.1 that $\hat{\beta} = 0.0$ is already sufficient for achieving an optimal order of convergence.

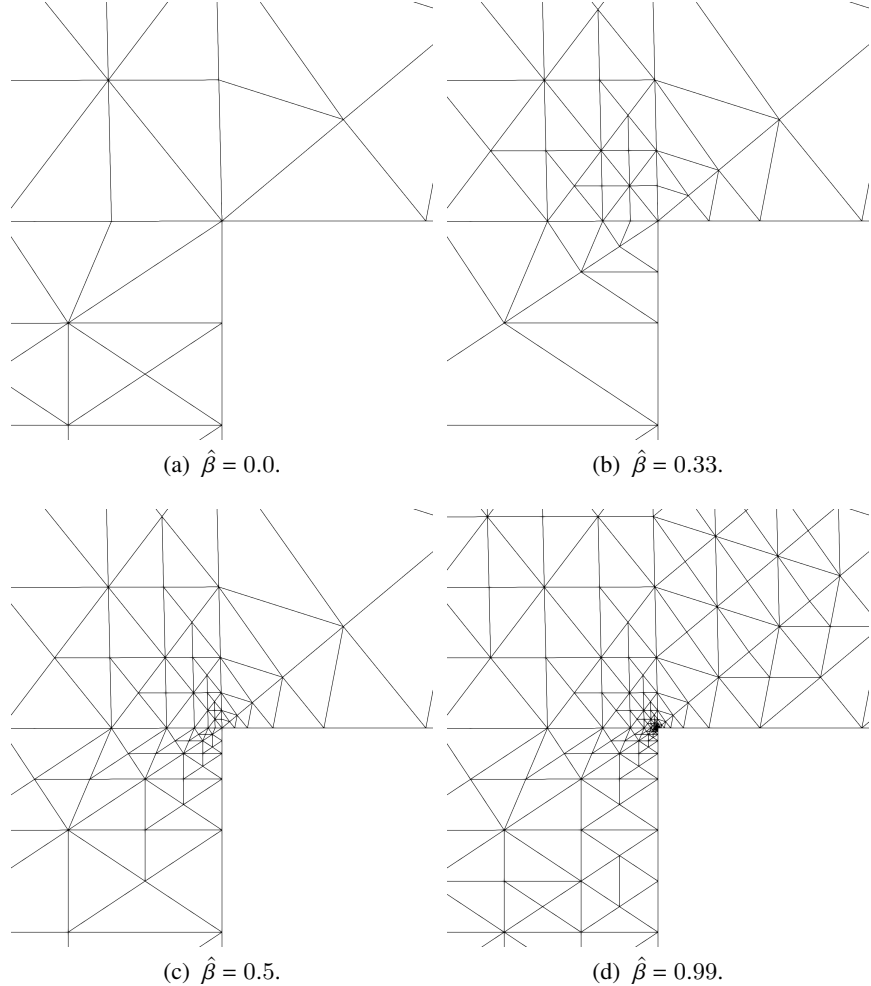


Figure 3: Mesh obtained via the L^2 a-posteriori bound (34) after 15 refinements.

4.2 r-adaptive strategy

The r-adaptive strategy aims to generate an adapted mesh \mathcal{T} by relocating a fixed number of mesh points. This process can be interpreted as the image from a computational domain Ω_c , having a fixed mesh \mathcal{T}_c , to a physical domain Ω , with variable mesh \mathcal{T}_i . The first method we propose is a variational one, where the transformation mapping is determined as the minimiser of an adaptation functional [BHR09; Win66]. The Moving Mesh PDE (MMPDE) associated with the minimiser will be solved by the Euler-Lagrange equation.

An adaptive mesh based on *Optimal Transport* will be also constructed in the last Subsection [BHR09]. This method exploits the strong dependence of the solution on the radial variable, which yields a mesh with high shape regularity and optimal convergence rate. A major advantage of the OT strategy is the computational efficiency, as the adapted mesh is obtained after solving a one dimensional algebraic equation for each node. On the contrary, the implementation of the former r-adaptive method requires a more computationally expensive iterative procedure.

4.2.1 Winslow's diffusion method

The Winslow' diffusion method is defined by the smooth mapping $\vec{x} = (x, y) = \vec{x}(\vec{\xi}) : \Omega_c \rightarrow \Omega$ or the inverse coordinate transformation $\vec{\xi} = (\xi, \eta) = \vec{\xi}(\vec{x}) : \Omega \rightarrow \Omega_c$. Practically, most of the MMPDEs were developed in terms of the inverse coordinate transformation, as this guarantees existence and uniqueness of the solution [Win66; Dvi91]. Thus, we will first solve the MMPDE associated with $\vec{\xi}(\vec{x})$ and the determine the transformed coordinate $\vec{x}(\vec{\xi})$ by change of variable. Consider the functional

$$I_{Win}[\vec{\xi}] = \frac{1}{2} \int_{\Omega} \frac{1}{w(\vec{x})} \sum_i (\nabla \xi_i)^T (\nabla \xi_i) d\vec{x}, \quad (39)$$

where $w(\vec{x}) > 0$ is a given monitor function. This function can be chosen to depend on the solution $u_h(\vec{x})$ of the physical PDE. We consider as possible choices:

1. Gradient:

$$w|_K = \left(1 + \frac{1}{\delta} |\nabla_h u_h|^2 \right)^{1/2} \quad (40)$$

2. Curvature:

$$w|_K = \left(1 + \frac{1}{\delta} |\Delta_h u_h| \right)^{1/2} \quad (41)$$

3. A-posteriori:

$$w|_K = \left(1 + \frac{1}{\delta} \eta_K^2 \right)^{1/2} \quad (42)$$

where δ is a prescribed intensity parameter for \mathcal{T} [HR11; BHR09]. The MMPDE associated with the functional (39) becomes

$$\partial_s \vec{x}(\vec{\xi}, s) = - \sum_{i=1} \vec{a}_i \nabla \cdot (\vec{M}^{-1} \vec{a}^i), \quad (43)$$

where s denotes the temporal variable, $\vec{a}^i = \nabla \xi_i$, $\vec{a}_i = \partial \vec{x} / \partial \xi_i$, and $\vec{M} = w(\vec{x}) I_2$ is the metric function. The replacement of the previous terms in the two-dimensional space gives

$$\begin{aligned} \partial_s \vec{x}(\vec{\xi}, s) = & \frac{1}{J^2 w^2} \left[(x_\eta^2 + y_\eta^2) \frac{\partial}{\partial \xi} \left(w \frac{\partial \vec{x}}{\partial \xi} \right) - (x_\xi x_\eta + y_\xi y_\eta) \frac{\partial}{\partial \eta} \left(w \frac{\partial \vec{x}}{\partial \xi} \right) \right. \\ & \left. - (x_\xi x_\eta + y_\xi y_\eta) \frac{\partial}{\partial \xi} \left(w \frac{\partial \vec{x}}{\partial \eta} \right) + (x_\xi^2 + y_\xi^2) \frac{\partial}{\partial \eta} \left(w \frac{\partial \vec{x}}{\partial \eta} \right) \right]. \end{aligned} \quad (44)$$

This PDE allows us to compute $\vec{x}(\vec{\xi}, s_{i+1})$ and hence \mathcal{T}_{i+1} given the knowledge of $w(\vec{x})$ and \mathcal{T}_c . Equation (44) is discretised in space using the FEM with linear Lagrangian elements and in time with the semi-implicit Euler method. To that purpose, we divide the temporal domain $[0, S]$ into a partition of N_S consecutive subintervals $0 = s_0 < s_1 < \dots < s_{N_S} = S$ with $s_i - s_{i-1} = k$ for all i . We treat the non-linear terms through evaluation at the current time step s_i , while the linear terms are evaluated at the next time step s_{i+1} .

Dirichlet boundary condition are imposed on all the edges except for that ones intersecting at the re-entrant corner. For those, the monitor function $w(\vec{\xi})$ has been first projected onto the two sides and the solution of the MMPDE5 [HR11] in one dimension is computed. This results in the movement of the mesh points towards the origin.

The non-convex domain Ω poses a practical complication for the application of Winslow's MMPDE. In fact, it is well known that if the computational domain Ω_c is not convex, the resulting physical mesh might feature very skewed or even overlapping elements. A natural solution for that issue is to define a computational mesh that is convex and solve for the coordinate transformation $\vec{x}(\vec{\xi})$ on this domain [WWR99; LTZ01]. Once Ω_c is selected, a mesh \mathcal{T}_c with the same topology as \mathcal{T} can be constructed by first specifying a correspondence between the boundaries $\partial\Omega$ and $\partial\Omega_c$ by a mapping $g(\vec{x})$ and then let \mathcal{T}_c be the image of \mathcal{T} under the mapping $\vec{\xi}(\vec{x})$ satisfying

$$\begin{aligned}\Delta\vec{\xi}(\vec{x}) &= 0 \text{ in } \Omega \\ \vec{\xi} &= g(\vec{x}) \text{ on } \partial\Omega.\end{aligned}\tag{45}$$

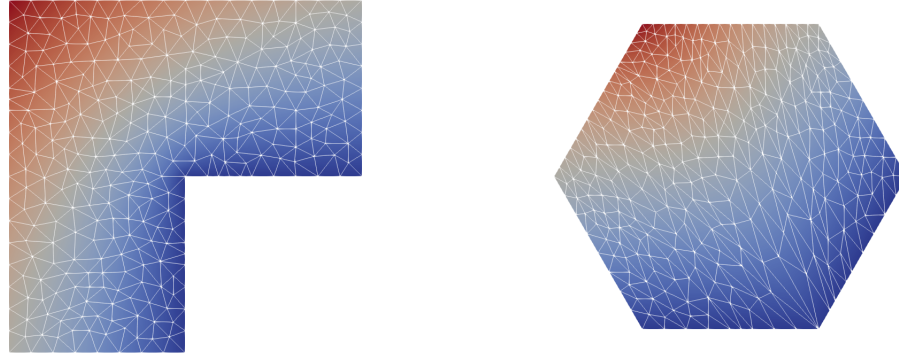


Figure 4: Solution of eq.(36) represented in the physical and computational domain.

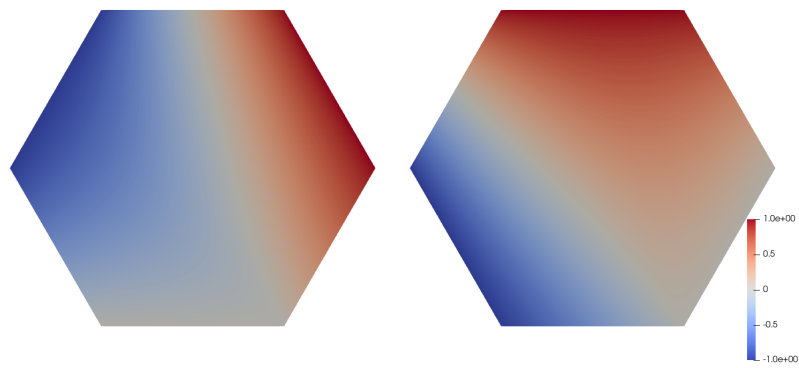


Figure 5: x and y coordinates represented in the computational mesh \mathcal{T}_c , obtained as solution of eq.(45). The boundary conditions match with that ones of the physical domain.

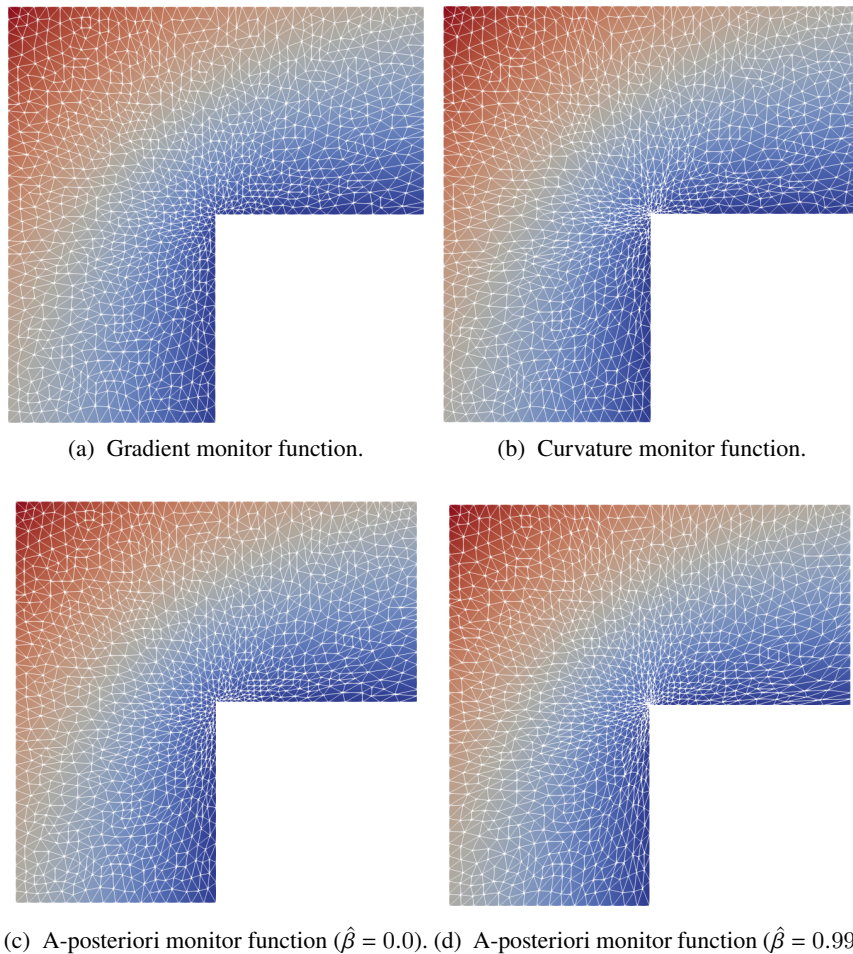


Figure 6: Solution of eq.(36) with mesh given by the Winslow's MMPDE (dim $\mathbb{V} = 7005$).

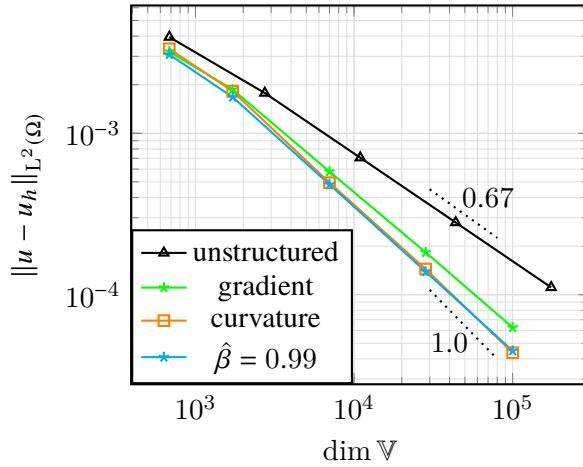


Figure 7: Asymptotic convergence rates for the Winslow's MMPDE for different monitor functions w (40)-(42).

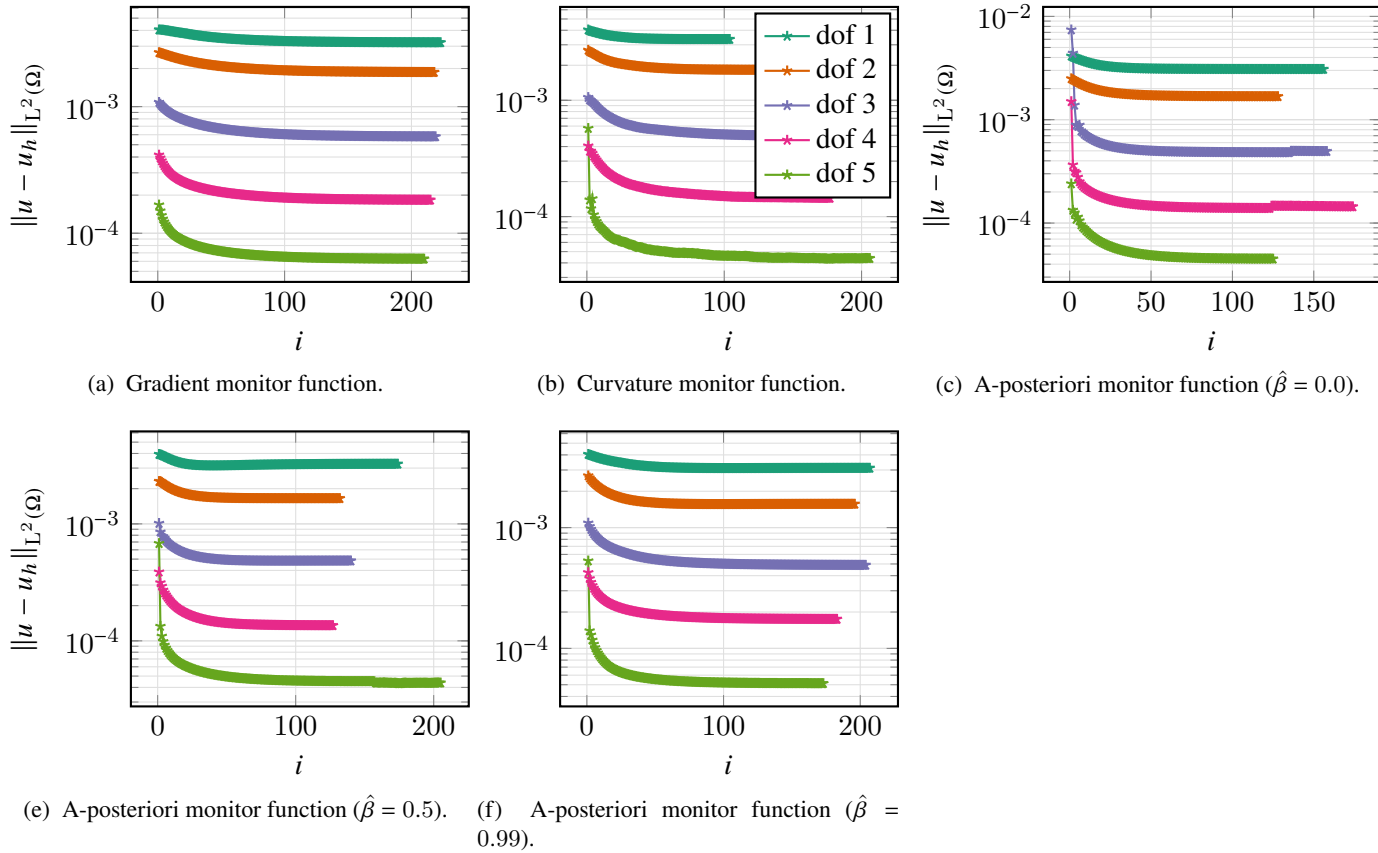


Figure 8: The solution error decreases monotonically over the iterations until reaching convergence for all the monitor functions. The relative tolerance has been fixed to 1×10^{-5} , while the timestep has been set to $k = 10^{-3}$. The degrees of freedom in the legend are 684, 1716, 7005, 28290, and 100080.

4.2.2 Optimal Transport mesh

We devise a mesh for the L-shaped region by solving the Monge-Ampère equation close to the re-entrant corner. The solution is then tuned to match the boundary of the domain.

Local mesh scaling Consider the general solution of equation (36). We know that the interpolation error of the solution for piecewise linear element can be bounded in the L^2 norm by $E_{max} \sim h^2 r^{\pi/\omega-2}$, where h is the local mesh size of an element close to the corner and r is the distance from the re-entrant corner, placed at the origin of \mathbb{R}^2 .

Following the *equidistribution principle*, we impose $E_{max} = 1$, so that we obtain $h \sim r^\gamma$, where $\gamma = 1 - \frac{\pi}{2\omega}$. Given the computation variable s , which represent the distance from the origin in the computational domain $\Omega_c \equiv \Omega$, we can interpret h as being proportional to dr/ds . Solving the differential equation $\frac{dr}{ds} = h = r^\gamma$ we obtain that $r \sim s^{\frac{1}{1-\gamma}}$.

Solution of Monge-Ampère equation We now look for a radially symmetric transformation from the corner region to itself. We can assume a radial symmetry because the singular behaviour of the solution near the origin does not depend on the angle θ . More details on the application of approach can be found in [BRW15]. Locally, the first integral of the Monge-Ampère equation implies that r satisfies the Ordinary Differential Equation (ODE) in polar coordinates

$$m(r)r dr d\theta = s ds d\theta, \quad (46)$$

where $m(r) = r^{-2\gamma}$ is the monitor function, which will be determined by the *a-priori* estimate for the interpolation error.

We expect that for large r the adapted mesh is almost regular. we then expect that $m(r) \sim 1$ far from the corner and consider the general expression

$$m(r) = A + Br^{-2\gamma}, \quad \alpha, \beta \in \mathbb{R} \quad (47)$$

From (46) we integrate over the variable θ and obtain

$$\left(A + Br^{-2\gamma} \right) r \frac{dr}{ds} = s,$$

so that r satisfies the nonlinear algebraic equation

$$Ar^2 + \frac{B}{1-\gamma}r^{2(1-\gamma)} = s^2. \quad (48)$$

The equation (48) then determines the mesh transformation. Note that the parameter A and B controls the level of mesh compression near the corner. In fact, for high values of B and small r we have $r \sim s^{1/(1-\gamma)}$ and for large A and r we have $r \sim s$. For the remainder of the analysis, we choose $B = (1 - \gamma)$, as this is the maximum admissible value that respects the boundary condition $A + B/(1 - \gamma) = 1$ when $r, s = 1$.

Computation of the OT mesh Suppose we have a uniform regular mesh $(\xi_{i,j}, \eta_{i,j})$ in Ω_c which we want to map to an adapted non uniform mesh $(x_{i,j}, y_{i,j})$ in the physical domain, with $i, j = 1, \dots, N$. The application of the Monge-Ampère method provides the desired mesh as follows:

1. For each pair (i, j) compute $s_{i,j}^2 = \xi_{i,j}^2 + \eta_{i,j}^2$
2. Compute the angle $\theta_{i,j}$ with respect to the semi-positive x axis by $\arctan\left(\frac{\eta_{i,j}}{\xi_{i,j}}\right)$.
3. Compute the length $l_{i,j}$ of the line spanned from the origin with angle $\theta_{i,j}$ to the boundary of the L-shaped domain.
4. Set the parameter $B = 1 - \gamma$ and enforce the condition $A + \frac{B}{1-\gamma}l_{i,j}^{-2\gamma} = 1$. This ensures that the new mesh boundary matches with the original boundary region.
5. Solve equation (48) to find $r_{i,j}$

6. Set $(x_{i,j}, y_{i,j}) = \frac{r_{i,j}}{s_{i,j}}(\xi_{i,j}, \eta_{i,j})$.

Given the new mesh $(x_{i,j}, y_{i,j})$, we can increase the dofs by uniform refinement or by applying the previous procedure from a more graded uniform mesh. The first approach is less computationally expensive and provides higher accuracy.

OT mesh for different γ In this Section, we show how the parameter γ affects the accuracy and the quality of the resulting OT mesh.

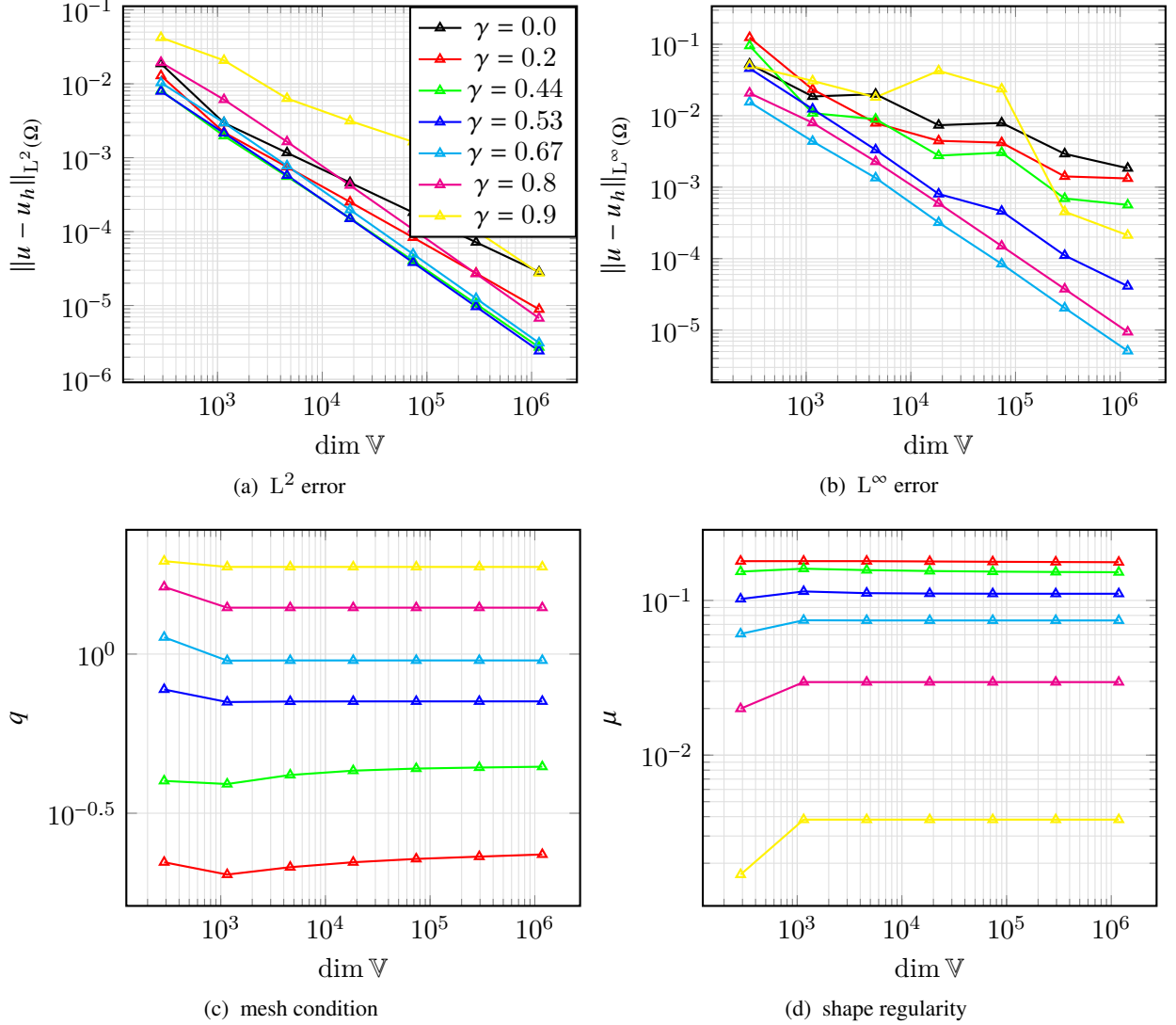


Figure 9: Error and quality measure of the OT mesh for different γ .

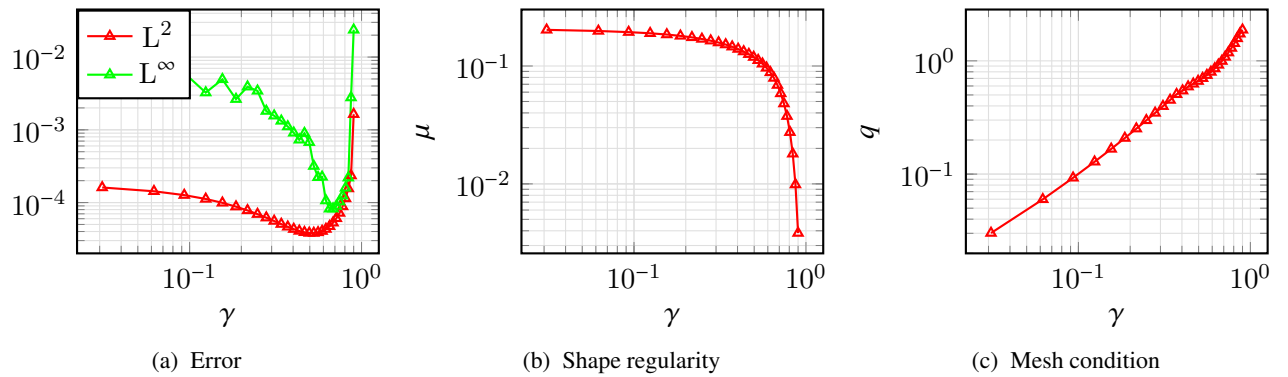


Figure 10: Error and quality measures for the a-priori OT mesh as function of γ ($\dim \mathbb{V} = 73728$).

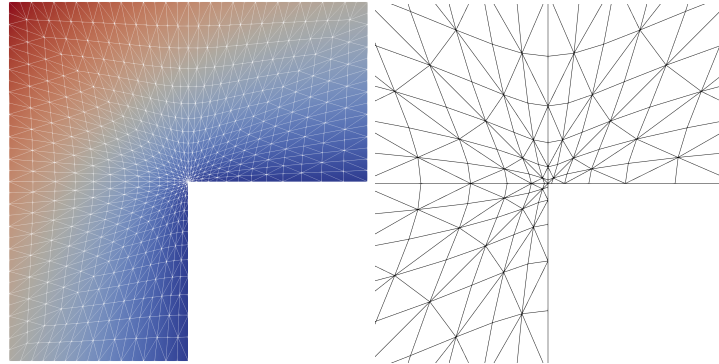


Figure 11: (Left) Solution of eq.(36) on the OT mesh with $\gamma = 0.53$. (Right) Zoom of the OT mesh on the re-entrant corner.

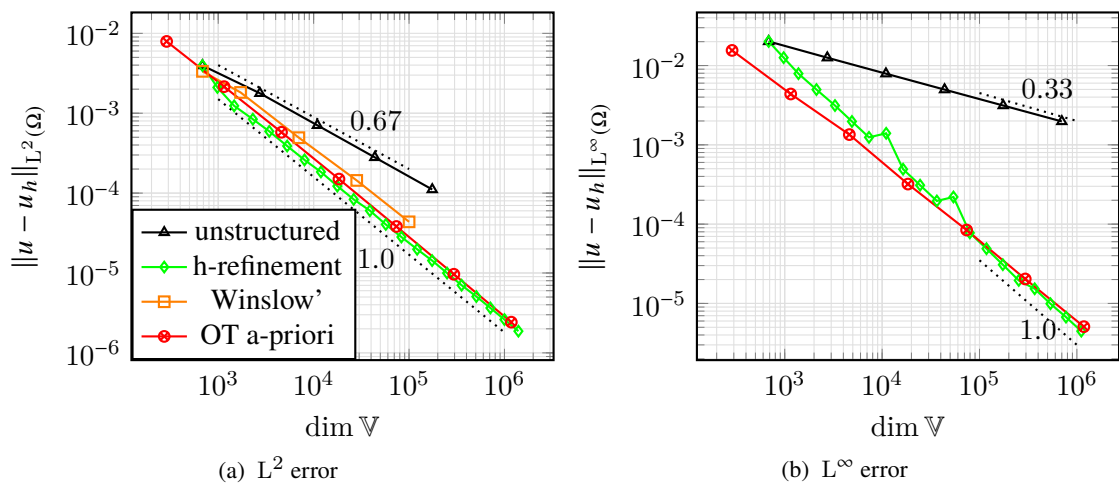


Figure 12: Asymptotic convergence rates for different adaptive strategies. Note that the rate of convergence is optimal for h-refinement and the OT strategy ($\gamma = 0.53, 0.67$ for L^2 and L^∞ norm, respectively).

Link between OT mesh and a-posteriori measure In this section we analyse the relationship between the a-posteriori bound η_K used for h-adaptivity and the OT mesh obtained by solving the one dimensional Monge-Ampère equation.

We note that the process of h-refinement aims at equidistributing η_K throughout each cell of the mesh by reducing the element mesh size through bisection. The a-posteriori measure can be then thought of as a monitor function. We then expect that η_K is constant in each cell generated by the OT algorithm in the vicinity of the origin.

The measure η_K has been computed from the OT mesh with $\dim \mathbb{V} = 7 \times 10^4$ as a function of the distance from the re-entrant corner. The plots clearly show the equidistribution obtained for the value γ yielding the highest accuracy in 12a and 12b.

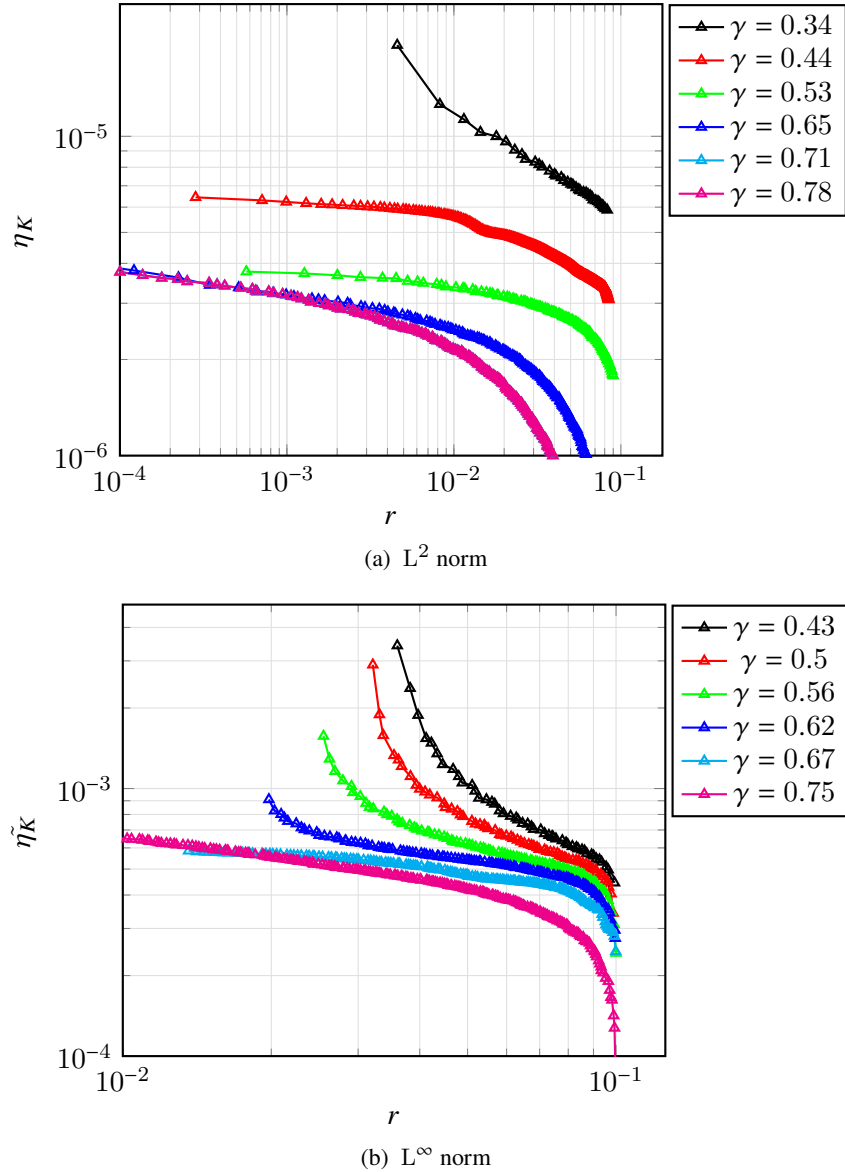


Figure 13: a-posteriori measure from OT mesh.

4.3 Crack domain

Let Ω be the domain with a crack $(-1, 1) \times (1, 1) / (([0, 1] \times \{0\}))$. The solution of Equation 36 is

$$u(r, \theta) = r^{1/2} \sin(\theta/2) \quad (49)$$

Numerically, the interior angle ω has been set to $2\pi - \epsilon$, with $\epsilon = 10^{-3}$.

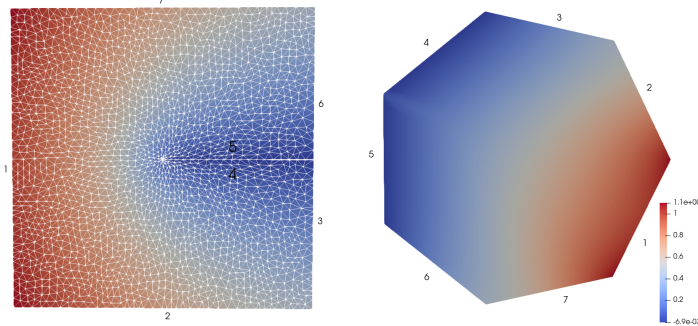


Figure 14: (Left) Solution of the Poisson eq. 49 via the Winslow' MMPDE. (Right) The computational domain Ω_c for the MMPDE (43).

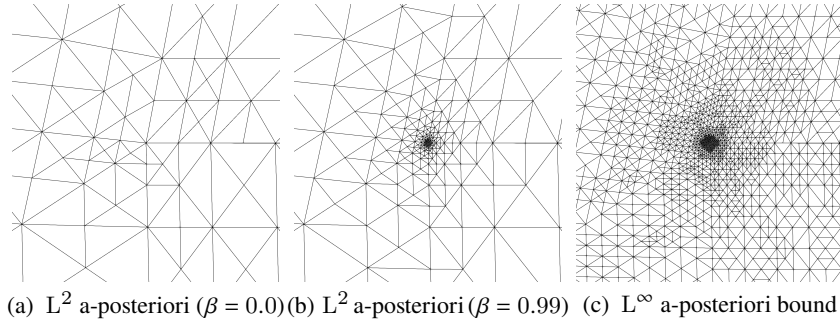


Figure 15: Zoom of the mesh near the re-entrant corner obtained with the a-posteriori bounds (34)-(35).

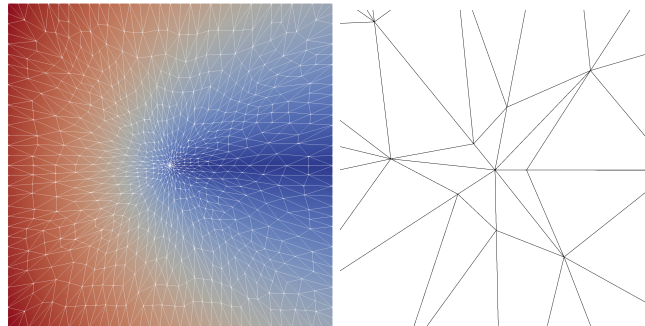


Figure 16: (Left) Solution of the Poisson eq. 49. (Right) Zoom of the OT mesh near the origin.

OT mesh for different γ In this Section, we show how the parameter γ , introduced in 4.2.2, affects the accuracy and the quality of the resulting OT mesh.

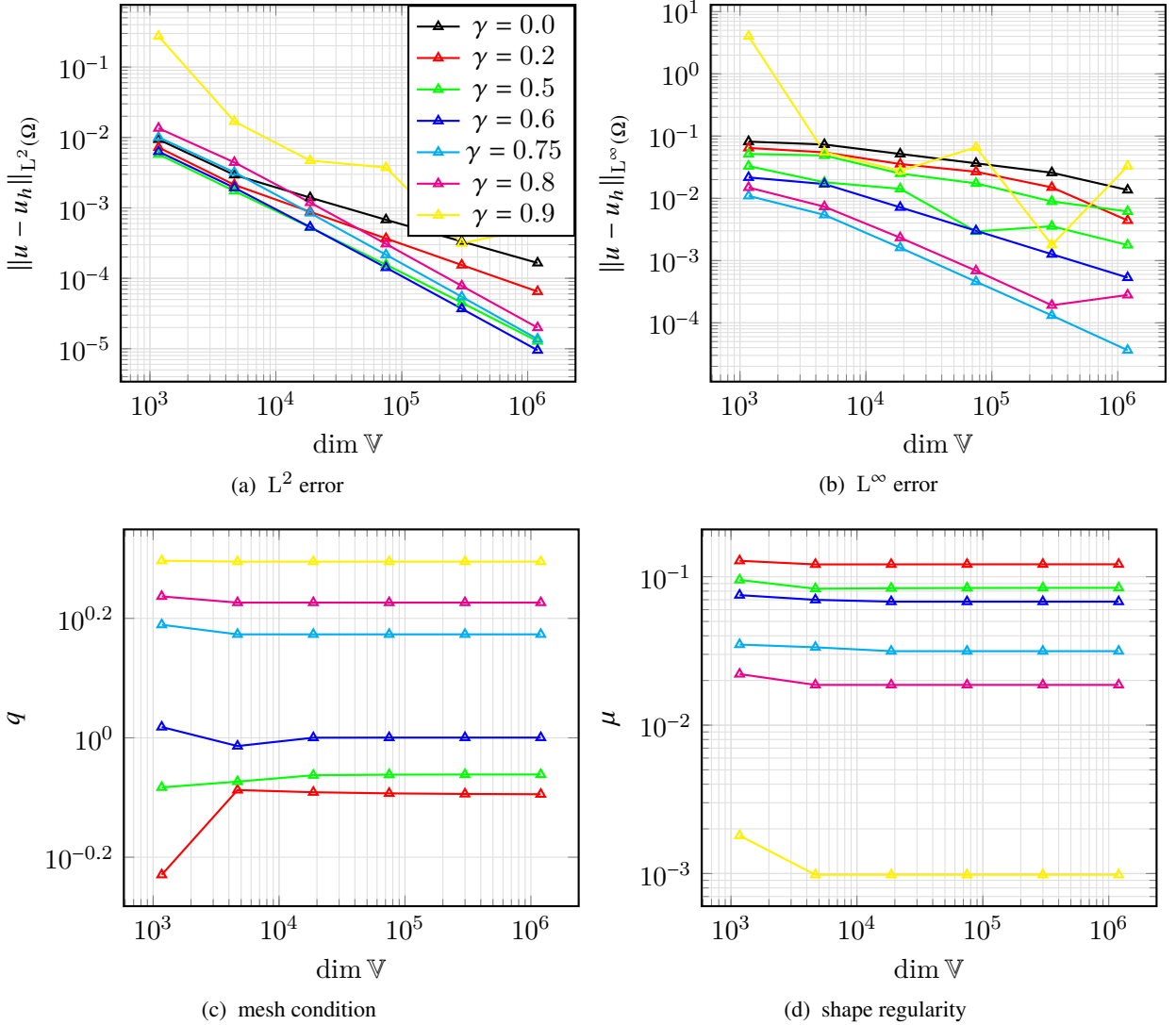


Figure 17: Error and quality measure for OT mesh for different γ .

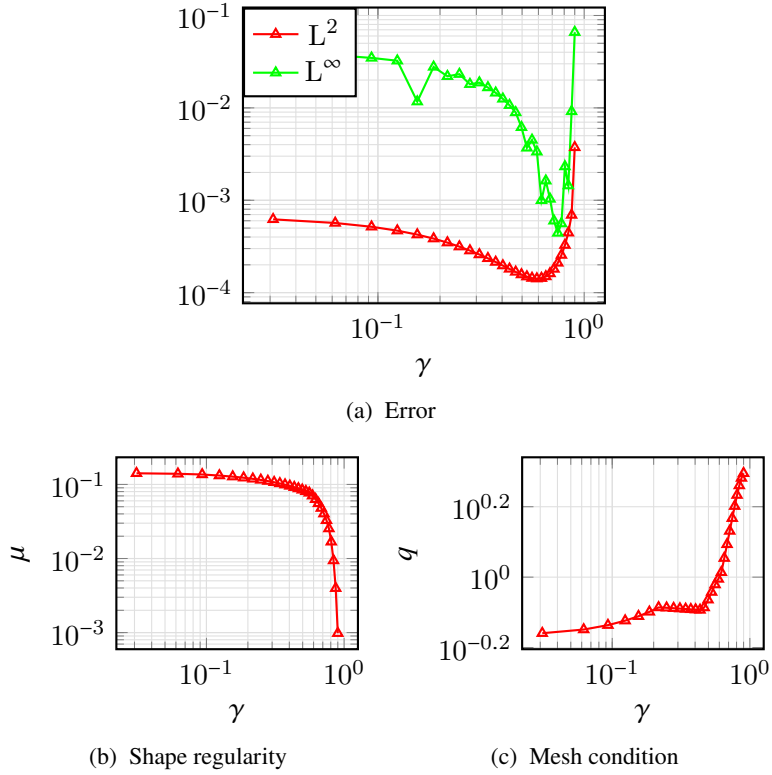


Figure 18: Error and quality measures for the a-priori OT mesh as function of γ ($\dim \mathbb{V} = 74880$).

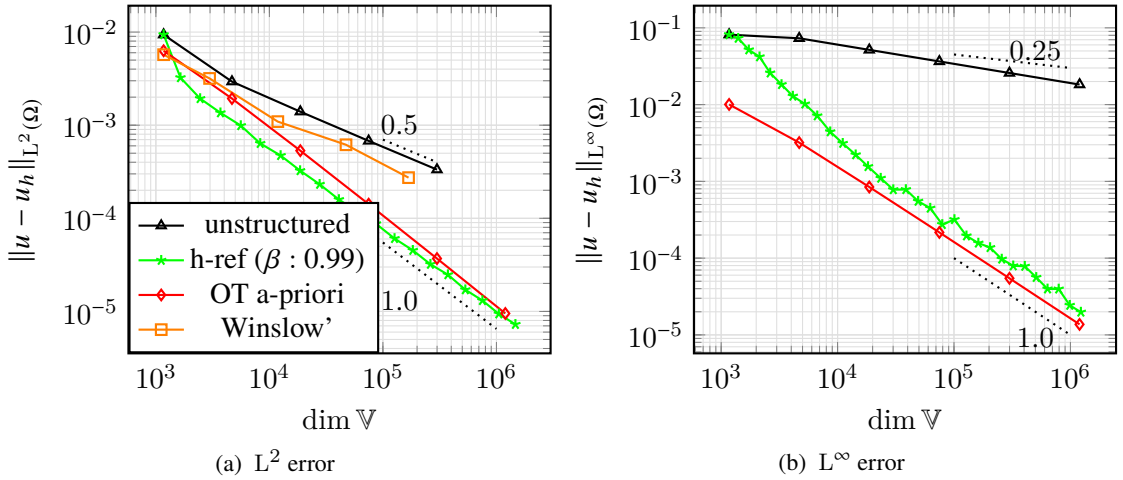


Figure 19: Asymptotic convergence rates for different adaptive strategies. Note that the rate of convergence is optimal for h-refinement and the OT strategy ($\gamma = 0.6, 0.75$ for L^2 and L^∞ norm, respectively).

Link between OT mesh and a-posteriori measure In this section we investigate the relationship between the a-posteriori bound η_K and the OT mesh as we did for the L-shaped domain. The plots evidence again that the estimator is equidistributed near the origin for the value of γ providing the highest accuracy.

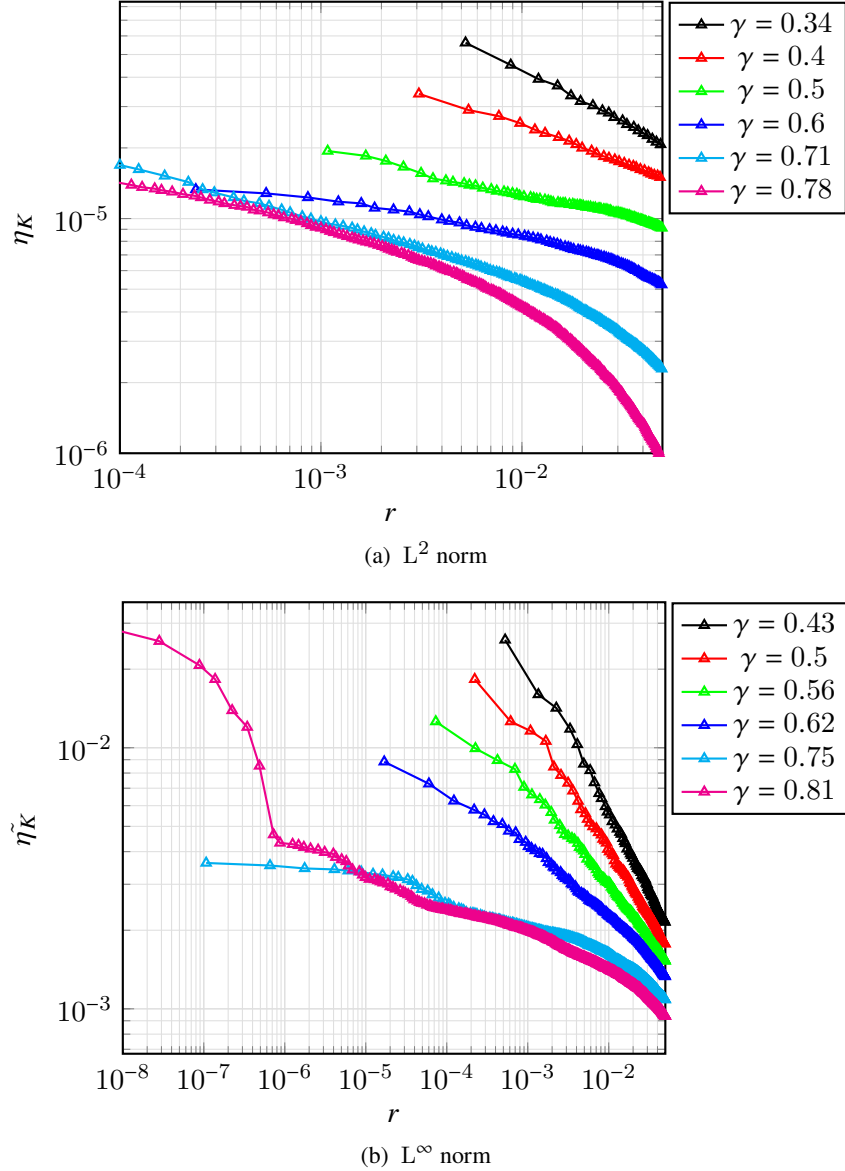


Figure 20: a-posteriori measure from OT mesh.

5 Mesh Skewness

The quality of the output mesh can be expressed in terms of different measures. Besides the shape regularity and mesh condition, a common metric used in the context of r-adaptive methods is the *skewness*, which indicates how far mesh elements are from being equilateral. A general indicator for triangular elements has been proposed in [BHR09] and employs the local map $Q_K : \hat{K} \rightarrow K$, with $\hat{K} \in \mathcal{T}_c$ and $K \in \mathcal{T}$. Given the corresponding Jacobian \mathbf{J}_K with eigenvalues λ_1 and λ_2 , the quality measure for the element K is defined as

$$Q_K := \frac{1}{2} \left(\frac{\lambda_1}{\lambda_2} + \frac{\lambda_2}{\lambda_1} \right). \quad (50)$$

We define the *global quality measure* as

$$Q = \max_{K \in \mathcal{T}} Q_K \quad (51)$$

Under the OT transformation $(x, y) = \frac{r}{s}(\xi, \eta)$ we can determine the value of Q analytically. As the mesh gets more uniform away from the corner, we assume that Q is given for cells where $r \sim 0$, so that the algebraic expression (48) simplifies to $r^{1-\gamma} = s$. We then compute the Jacobian of the map $(x, y) = s^{\frac{\gamma}{1-\gamma}}(\xi, \eta)$:

$$\mathbf{J} = \begin{bmatrix} x_\xi & x_\eta \\ y_\xi & y_\eta \end{bmatrix} = \frac{\gamma}{1-\gamma} (\xi^2 + \eta^2)^{\frac{\gamma}{2(1-\gamma)} - 1} \begin{bmatrix} \xi^2 + (\xi^2 + \eta^2)^{\frac{1-\gamma}{\gamma}} & \xi\eta \\ \xi\eta & \eta^2 + (\xi^2 + \eta^2)^{\frac{1-\gamma}{\gamma}} \end{bmatrix}$$

The eigenvalues are $\lambda_1 = \frac{1-\gamma}{\gamma}(\xi + \nu)^2$ and $\lambda_2 = \frac{1}{\gamma}(\xi + \nu)^2$. Finally, the skewness is expressed in terms of the coefficient γ by:

$$Q(\gamma) = \frac{1}{2} \left(\frac{\lambda_1}{\lambda_2} + \frac{\lambda_2}{\lambda_1} \right) = \frac{1}{2} \left((1-\gamma) + \frac{1}{(1-\gamma)} \right). \quad (52)$$

This shows that as γ increases, the mesh quality deteriorates. This is also qualitatively suggested by looking at the OT mesh produced for the L-shaped and the crack domain (11)-(16).

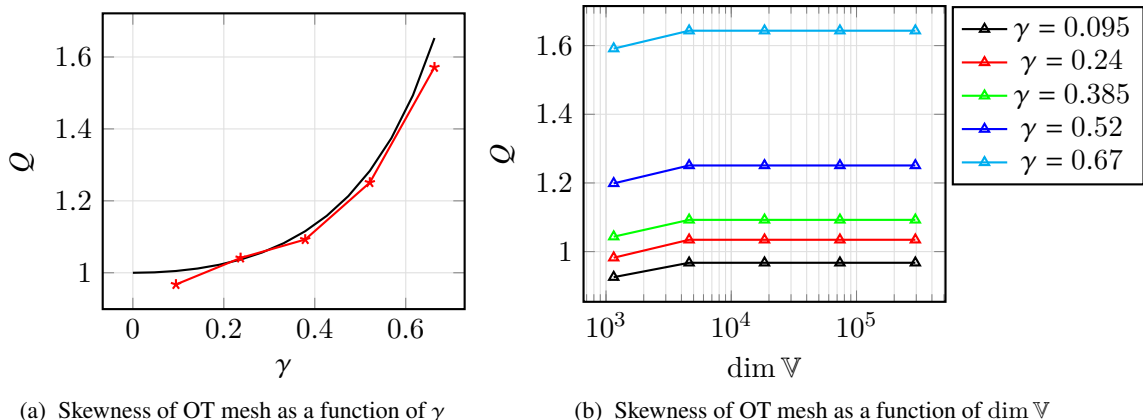


Figure 21: (Left) We show that the dependence of the skewness measure on γ computed numerically fits the theoretical formula in (22). (Right) The value of $Q(\gamma)$ is independent on the dimension of the FE space.

6 Conclusions

In this paper, we have analysed the properties of different h - and r -adaptive mesh strategies for the solution of the Poisson equation on two non-convex domains. We first derived the SIP-dG variational formulation using the theoretical framework of the weighted Sobolev spaces. We stated the Theorem of existence and uniqueness of the solution under a condition for the parameter β_{min} , which relates to the amplitude of the re-entrant corners.

Our first contribution consisted in the derivation of an *a-posteriori* error upper bound for the SIP-dG method in the L^2 norm. This has showed optimal order of convergence independently on the parameter $\hat{\beta}$, leading to the hypothesis that it does not directly affect β_{min} . The same optimal order of convergence has been achieved in the L^∞ norm with the corresponding a-posteriori estimator.

Concerning the moving mesh methods, we first conducted numerical tests on the *Winslow's* MMPDE for three different monitor functions, with that one based on the a-posteriori bound yielding the best accuracy. This should encourage the research community involved in Variational-based moving mesh methods to adopt a model-dependent monitor function, provided that an a-posteriori indicator is available.

An algorithm for the generation of an *Optimal Transport*-based mesh has also been presented. The method produces a mesh outperforms the MMPDE, yielding optimal asymptotic convergence rate in both L^2 and L^∞ norm.

We have shown numerical evidence of the optimal expression for obtaining the OT mesh for both domains and norms. A further study has also evidenced that the optimality in terms of accuracy and convergence rate guarantees equidistribution of the a-posteriori bound for the corresponding norm.

We have introduced the *skewness* as an alternative quality measure for r.adaptive methods and showed both theoretically and numerically that this increases only as a function of the interior re-entrant angle and is independent on the dimensione of the FE space.

In conclusion, we have established that the L^2 and L^∞ a-posteriori estimator provides optimal order of convergence for h -refinement. We also showed that those estimators are equidistributed on the optimal OT mesh (in terms of accuracy). Lastly, we have proved and showed numerically that the skewness of the OT mesh does only depend on the interior angle.

In the view of the above considerations, our future research directions will examine:

1. Application of the numerical procedure on polygons with multiple re-entrant cornerns and to other relevant time-dependent problems arising in physics, such as the Shallow-Water equations;
2. Investigation on the relationship between different mesh quality measures;
3. Scalability of the algorithms through parallelisation;
4. Extension of the OT strategy by solving a Monge-Ampère type equation [BRW15].

References

- [Win66] A.M. Winslow. “Numerical solution of the quasilinear poisson equation in a nonuniform triangle mesh”. In: *Journal of Computational Physics* 1.2 (1966), pp. 149–172.
- [BR72] I. Babuška and M.B. Rosenzweig. “A Finite Element Scheme for Domains with Corners”. In: *Numer. Math.* 20.1 (1972), pp. 1–21.
- [BKP79] I. Babuška, R.B. Kellogg, and J. Pitkäranta. “Direct and Inverse Error Estimates for Finite Elements with Mesh Refinements”. In: *Numer. Math.* 33.4 (1979), pp. 447–471.
- [Arn82] D. Arnold. “An Interior Penalty Finite Element Method with Discontinuous Elements”. In: *SIAM Journal on Numerical Analysis* 19.4 (1982), pp. 742–760.

- [BG88] I. Babuška and B.Q. Guo. “Regularity of the Solution of Elliptic Problems with Piecewise Analytic Data. Part I. Boundary Value Problems for Linear Elliptic Equation of Second Order”. In: *SIAM Journal on Mathematical Analysis* 19.1 (1988), pp. 172–203.
- [BG89] I. Babuška and B. Q. Guo. “Regularity of the Solution of Elliptic Problems with Piecewise Analytic Data. II: The Trace Spaces and Application to the Boundary Value Problems with Nonhomogeneous Boundary Conditions”. In: *SIAM Journal on Mathematical Analysis* 20.4 (1989), pp. 763–781.
- [Dvi91] A.S. Dvinsky. “Adaptive grid generation from harmonic maps on Riemannian manifolds”. In: *Journal of Computational Physics* 95.2 (1991), pp. 450–476.
- [CC98] B. Cockburn and S. Chi Wang. “The Local Discontinuous Galerkin Method for Time-Dependent Convection-Diffusion Systems”. In: *SIAM Journal on Numerical Analysis* 35.6 (1998), pp. 2440–2463.
- [Sch98] C. Schwab. *p-and hp-finite element methods: Theory and applications in solid and fluid mechanics*. Oxford University Press, 1998.
- [WWR99] C. Weiming, H. Weizhang, and D.R. Robert. “An r -Adaptive Finite Element Method Based upon Moving Mesh PDEs”. In: *Journal of Computational Physics* 149.2 (1999), pp. 221–244.
- [Arn+00] D. Arnold et al. “Discontinuous Galerkin Methods”. In: vol. 11. 2000, pp. 89–101.
- [CC01] B. Cockburn and S. Chi Wang. In: *Journal of Scientific Computing* 16 (2001), pp. 173–261.
- [LTZ01] R. Li, T. Tang, and P. Zhang. “Moving Mesh Methods in Multiple Dimensions Based on Harmonic Maps”. In: *Journal of Computational Physics* 170.2 (2001), pp. 562–588.
- [Arn+02] D. Arnold et al. “Unified Analysis of Discontinuous Galerkin Methods for Elliptic Problems”. In: *SIAM J. Numer. Anal.* 39 (2002).
- [ZS02] C. Zhiqiang and K. Seokchan. “A Finite Element Method Using Singular Functions for the Poisson Equation: Corner Singularities”. In: *SIAM Journal on Numerical Analysis* 39.1 (2002), pp. 286–299.
- [ZSG02] C. Zhiqiang, K. Seokchan, and W. Gyungsoo. “A finite element method using singular functions for the Poisson equation: crack singularities”. In: *Numerical Linear Algebra with Applications* 9.67 (2002), pp. 445–455.
- [Wih03] T. Wihler. “Discontinuous Galerkin FEM for elliptic problems in polygonal domains”. PhD thesis. 2003.
- [BS08] S.C. Brenner and L.R. Scott. *The Mathematical Theory of Finite Element Methods*. Vol. 15. Texts in Applied Mathematics. Springer, 2008.
- [BHR09] C. Budd, W. Huang, and R. Russell. “Adaptivity with moving grids”. In: *Acta Numerica* 18 (2009), pp. 111–241.
- [LW10] A. Logg and G.N. Wells. “DOLFIN”. In: *ACM Transactions on Mathematical Software* 37.2 (2010), pp. 1–28.
- [HR11] W. Huang and R. Russell. *Adaptive Moving Mesh Methods*. Vol. 174. 2011.
- [DG12] A. Demlow and E. H. Georgoulis. “Pointwise a Posteriori Error Control for Discontinuous Galerkin Methods for Elliptic Problems”. In: *SIAM Journal on Numerical Analysis* 50.5 (2012), pp. 2159–2181.

- [BRW15] C.J. Budd, R.D. Russell, and E. Walsh. “The geometry of r -adaptive meshes generated using optimal transport methods”. In: *Journal of Computational Physics* 282 (2015), pp. 113–137.
- [SH16] K. Seokchan and L. Hyung-Chun. “A finite element method for computing accurate solutions for Poisson equations with corner singularities using the stress intensity factor”. In: *Computers and Mathematics with Applications* 71.11 (2016), pp. 2330–2337.
- [GMP17] E. Georgoulis, C. Makridakis, and T. Pryer. “Babuška-Osborn techniques in discontinuous Galerkin methods: L^2 -norm error estimates for unstructured meshes”. In: *arXiv:1704.05238* (2017).
- [EG21] Alexandre Ern and Jean-Luc Guermond. *Finite Elements I: Approximation and Interpolation*. 2021.

A Derivation of optimal γ for L^∞ and L^2 norm

A.1 L^∞ norm

We derive here the optimal value of the exponent γ that minimises the L^∞ norm. We consider the function $u(r) = r^\alpha$, where α is a parameter that depends on the interior angle of the re-entrant corner. As $\alpha < 1$ and $u \notin C^2[0, 1]$, we must split the error analysis into two parts. Then, we write

$$\|u - p_{1,N}\|_{\infty, [0,1]} = \max\{\|u - p_{1,N}\|_{\infty, [0,x_1]}, \|u - p_{1,N}\|_{\infty, [x_1,1]}\}$$

For the first part, by triangle inequality

$$\|u - p_{1,N}\|_{\infty, [0,x_1]} \leq \|u\|_{\infty, [0,x_1]} + \|p_{1,N}\|_{\infty, [0,x_1]} = x_1^\alpha + p_{1,N}(x_1) = 2 \left(\left(\frac{1}{N} \right)^\beta \right)^\alpha = 2N^{-\alpha\beta}, \quad (53)$$

using the fact that both u and $p_{1,N}$ is an increasing function.

We treat each interval $[x_{j-1}, x_j]$ for $j \geq 2$ separately. For $h_j = x_j - x_{j-1}$, we have

$$\|u - p_{1,N}\|_{\infty, [x_{j-1}, x_j]} \leq \frac{1}{8} h_j^2 \|u''\|_{\infty, [x_{j-1}, x_j]},$$

with

$$\|u''\|_{\infty, [x_{j-1}, x_j]} = \sup_{[x_{j-1}, x_j]} |u''| = |u''(x_{j-1})| = |\alpha(\alpha-1)| x_{j-1}^{\alpha-2} = |\alpha(\alpha-1)| \left(\frac{j-1}{N} \right)^{\beta(\alpha-2)}.$$

Using the mean-value theorem for the increasing function $g(t) = t^\beta$ on the interval $t_j \in [(j-1)/N, j/N]$ we have

$$h_j = x_j - x_{j-1} = g(j) - g(j-1) = [j - (j-1)] g'(t_j) = \frac{1}{N} \beta \left(\frac{t_j}{N} \right)^{\beta-1} \leq \frac{\beta}{N} \left(\frac{j}{N} \right)^{\beta-1}.$$

We then obtain

$$\begin{aligned} \|u - p_{1,N}\|_{\infty, [x_{j-1}, x_j]} &\leq \frac{1}{8} \left[\frac{\beta}{N} \left(\frac{j}{N} \right)^{\beta-1} \right]^2 |\alpha(\alpha-1)| \left(\frac{j-1}{N} \right)^{\beta(\alpha-2)} \\ &= \frac{|\alpha(\alpha-1)|}{8} \beta^2 N^{-\alpha\beta} \left(\frac{j^{2(\beta-1)}}{(j-1)^{\beta(2-\alpha)}} \right) \end{aligned} \quad (54)$$

Finally, Eqs. (53) and (54) give

$$\|u - p_{1,N}\|_{\infty, [0,1]} \leq \max_{j=1, \dots, N} \{\|u - p_{1,N}\|_{\infty, [x_{j-1}, x_j]}\} \leq N^{-\alpha\beta} \max_{j=2, \dots, N} \left\{ 2, \frac{|\alpha(\alpha-1)|}{8} \beta^2 \frac{j^{2(\beta-1)}}{(j-1)^{\beta(2-\alpha)}} \right\}.$$

By imposing $2(\beta-1) = \beta(2-\alpha) \Rightarrow \beta = 2/\alpha$ we obtain that the order of convergence for the L^∞ norm is N^{-2} .

If s is the computational variable for computing the OT mesh, then the L^∞ norm is equidistributed with $r = s^\beta$, so that $dr = \beta s^{\beta-1} ds$. Hence we have $m(r)s^\beta \beta s^{\beta-1} ds = sds \Rightarrow m(r) = 1/\beta(r^{1/\beta})^{2(1-\beta)} = cr^{-2\gamma}$.

In particular, for the L-shaped domain ($\alpha = 3/2$) we get that $\beta = 3$ and $\gamma = 2/3$, whereas for the crack domain ($\alpha = 1/2$) we get $\beta = 4$ and $\gamma = 3/4$. The results derived are in agreement with both Figure 9b and 17b.

A.2 L^2 norm

A.2.1 1D - case

Following the derivation in [HR11], the optimal mesh density function for piecewise linear interpolation in L^2 norm is

$$\rho = \left(1 + \frac{1}{\delta} |u''|^2\right)^{1/5}.$$

Ignoring the constant term θ , the equidistribution principle reads as $h\rho = C$ in the limit for $N \rightarrow \infty$; so since $|u''| = Kr^{\alpha-2}$

$$h = \frac{dr}{ds} = Kr^{(2-\alpha)\frac{2}{5}}$$

For the L-shaped domain, we have $\alpha = 2/3$ and $h = Kr^{8/15}$, with $\gamma = 8/15 \sim 0.53$. For the crack domain, we have $\alpha = 1/2$ and $h = Kr^{6/10}$, with $\gamma = 3/5$. These results are in agreement with Figure 9a and 17a.

A.2.2 2D - case

The local implementation of the OT plan discussed previously provides the optimal value of $\gamma = 0.53$, which provides the highest accuracy results. Another critical value can be obtained with a 2D argumentation; which gives an exponent that is close to the optimal value.

In order derive the critical γ for the 2D case, consider the transformation from the mesh element \hat{K} to the element K in the physical domain:

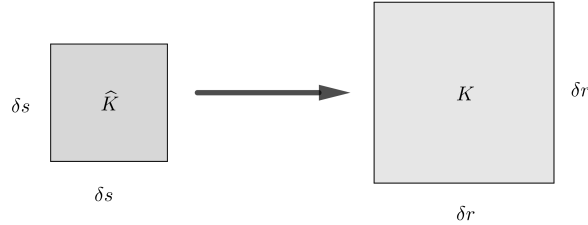


Figure 22: Map from Computational to Physical domain. By the mesh has constant skewness for fixed γ , so we can approximate K near the origin by a square.

If the solution $u \sim r^{2/3} f(\theta)$, the interpolation error is $\delta^2 r r^{2/3-2} f(\theta)$. The L_K^2 local estimate of the interpolation error is then proportional to:

$$L_K^2 \sim \delta r (\delta^2 r r^{2/3-2}) = \delta^3 r r^{-4/3}. \quad (55)$$

The equidistribution of this quantity leads to

$$\begin{aligned} \left(\frac{dr}{ds}\right)^3 r^{-4/3} &\sim const \Rightarrow r \sim s^{9/5} \Rightarrow s \sim r^{5/9} \\ m(r) &= \frac{s}{r} \frac{ds}{dr} = \frac{r^{5/9}}{r} r^{-4/9} = r^{-8/9}. \end{aligned} \quad (56)$$

This gives $\gamma = 4/9$ as the critical exponent. This result is not consistent with the optimal exponent of $\gamma = 0.53$. There might be multiple reasons why this occurs:

- The optimal exponent equidistributes the local a-posteriori estimate η_K (Fig. 13a), which provides a reliable estimate of the error due to the SIP-DG discretisation. The estimate η_K is evaluated along edges, so this can explain why the 1D derivation of the optimal monitor function yields the lowest L^2 error.

- The derivation of the critical exponent in the 2D case is based on the interpolation error and the assumption that the physical cell does not get skewed. The first criterion might justify the application for that γ in case the Poisson equation is solved using the Finite Difference or the Finite Element method, differently from the SIPD-dG framework adopted in this paper.
- The nodes of OT mesh for the L-shaped domain are equidistant to the origin () independently on the angular variable. This observation further suggests that in the neighbourhood of the origin the problem can be considered as 1D.